HHS Public Access

Author manuscript

Exp Mol Pathol. Author manuscript; available in PMC 2024 March 14.

Published in final edited form as:

Exp Mol Pathol. 2023 December ; 134: 104869. doi:10.1016/j.yexmp.2023.104869.

Inhibition of integrin alpha v/beta 5 mitigates the protective effect induced by irisin in hemorrhage

Lijiang Wang[a], **Supaporn Kulthinee**[a], **John Slate-Romano**[a], **Thomas Zhao**[d], **Hamsa Shanmugam**[a], **Patrycja M Dubielecka**[b], **Ling X. Zhang**[b], **Gangjian Qin**[c], **Shougang Zhuang**[b], **Y. Eugene Chin**[e], **Ting C. Zhao**[a,f,*]

[a]Department of Plastic Surgery, Rhode Island Hospital, Brown University, USA

[b]Department of Medicine, Rhode Island Hospital, Warren Alpert Medical School of Brown University, Providence, RI, USA

[c]Department of Biomedical Engineering, University of Alabama at Birmingham, Birmingham, AL, USA

[d]Boston University, Boston, MA, USA

[e]Soochow University, Suzhou, China

[f]Department of Surgery, Rhode Island Hospital, Brown University, Providence, RI, USA

Abstract

Introduction: Irisin plays an important role in regulating tissue stress, cardiac function, and inflammation. Integrin αvβ5 was recently identified as a receptor for irisin to elicit its physiologic function. It remains unknown whether integrin αvβ5 is required for irisin's function in modulating the physiologic response to hemorrhage. The objective of this study is to examine if integrin αvβ5 contributes to the effects of irisin during the hemorrhagic response.

Methods: Hemorrhage was induced in mice by achieving a mean arterial blood pressure of 35–45 mmHg for one hour, followed by two hours of resuscitation. Irisin (0.5 μg/kg) was administrated to assess its pharmacologic effects in hemorrhage. Cilengitide, a cyclic Arg-Gly-Asp peptide (cRGDyK) which is an inhibitor of integrin αvβ5, or control RGDS (1 mg/kg) was administered with irisin. In another cohort of mice, the irisin-induced protective effect was

*Corresponding author at: Brown University, Alpert Medical School, Department of Surgery, Department of Plastic and Reconstructive Surgery, Rhode Island Hospital, 593 Eddy Street, Providence, RI 02903, USA. Ting_Zhao@Brown.Edu (T.C. Zhao).

Submission declaration and verification

Submission of an article implies that the work described has not been published previously, that it is not under consideration for publication elsewhere, that its publication is approved by all authors and tacitly or explicitly by the responsible authorities where the work was carried out, and that, if accepted, it will not be published elsewhere in the same form, in English or in any other language, including electronically without the written consent of the copyright holder.

Author statement

Submission of an article implies that the work described has not been published previously, that it is not under consideration for publication elsewhere, that its publication is approved by all authors and tacitly or explicitly by the responsible authorities where the work was carried out, and that, if accepted, it will not be published elsewhere in the same form, in English or in any other language, including electronically without the written consent of the copyrightholder.

Declaration of Competing Interest

The authors declare that they have no competing interests.

examined after knocking down integrin β5 with nanoparticle delivery of integrin β5 sgRNA using CRSIPR/Cas-9 gene editing. Cardiac function and hemodynamics were measured using echocardiography and femoral artery catheterization, respectively. Systemic cytokine releases were measured using Enzyme-linked immunosorbent assay (ELISA). Histological analyses were used to determine tissue damage in myocardium, skeletal muscles, and lung tissues. Terminal deoxynucleotidyl transferase dUTP nick end labeling (TUNEL) was carried out to assess apoptosis in tissues.

Results: Hemorrhage induced reduction of integrin αvβ5 in skeletal muscles and repressed recovery of cardiac performance and hemodynamics. Irisin treatment led to significantly improved cardiac function, which was abrogated by treatment with Cilengitide or knockdown of integrin β5. Furthermore, irisin resulted in a marked suppression of tumor necrosis factor-α (TNF-α) and interleukin-1 (IL-1), muscle edema, and inflammatory cells infiltration in myocardium and skeletal muscles, which was attenuated by Cilengitide or knockdown of integrin β5. Irisin-induced reduction of apoptosis in the myocardium, skeletal muscles, and lung, which were attenuated by either the inhibition of integrin αvβ5, or knockdown of integrin β5.

Conclusion: Integrin αvβ5 plays an important role for irisin in modulating the protective effect during hemorrhage.

Keywords

Hemorrhage; Irisin; integrin αvβ5; Cardiac function; Organ failure; Stresses

1. Introduction

Hemorrhage, as a result of injury or trauma, can result in detrimental physiologic instability resulting in tissue injuries such as hypotension, tissue hypoxia, and acidosis (Torres et al., 2004). The initial physiologic response to hemorrhage is the activation of the sympathetic nervous system, which regulates cardiac performance and vasoconstriction to maintain blood pressure and preserve the perfusion of essential organs (Koyama et al., 1988; Skoog et al., 1985). This is closely associated with diminished cardiac function, multi-organ ischemia (Elansary et al., 2022; Kvarstein et al., 2003), and a triggered inflammatory cascade (Hierholzer et al., 1998). The inability to recover cardiac function following hemorrhage leads to cardiovascular collapse and mortality (Chatpun and Cabrales, 2011). Current treatments for hemorrhagic shock includes bleeding control and early volume repletion (Krausz, 2006), but advancements in cardiac resuscitation remain essential to improving treatment regimens.

Irisin, a 112 amino acid polypeptide that is proteolytically cleaved from the extracellular domain of fibronectin type III domain-containing protein 5 (FNDC5), has recently gained attention (Bilski et al., 2015; Boström et al., 2012; Huh et al., 2014). Muscle contractions during exercise cause increased transcription of peroxisome proliferator-activated receptor gamma co-activator (PGC-1α), which upregulates the expression of FNDC5, from which irisin is then cleaved (Bilski et al., 2015; Boström et al., 2012; Erickson, 2013; Huh et al., 2014; Kim et al., 2007; Schnyder and Handschin, 2015). The structure of irisin consists of a flexible tail composed of a disordered array of amino acids at the C-terminus and a dimer

of two adjacent antiparallel fibronectin-III domains at the N-terminus (Schumacher et al., 2013), which facilitates the ability of irisin to act as a ligand and bind receptors (Schumacher et al., 2013).

Irisin is generated primarily in skeletal muscles, but has also been found to be produced by white adipose tissue and the heart (Boström et al., 2012; Gaggini et al., 2017; Polyzos et al., 2018; Roca-Rivada et al., 2013; Wrann et al., 2013). Previous studies have demonstrated that irisin exerts protective effects for cardiac tissue during sepsis and ischemic cardiomyopathy and blunts the inflammatory processes (Matsuo et al., 2015; Ouyang et al., 2020; Pan et al., 2021). Irisin has been found to have anti-inflammatory and antioxidant effects which may help reduce the extent of tissue damage caused by hemorrhage (Li et al., 2021c; Slate-Romano et al., 2022; Zhu et al., 2021). Our previous study demonstrated a significant reduction in the amount of irisin in mice exposed to hemorrhage, and that the treatment of these mice with irisin resulted in improved insulin resistance (Kulthinee et al., 2022).

Integrins are dimeric cell-surface receptors composed of α and β subunits (Hynes, 2002; Lacy-Hulbert et al., 2007). The αv subunit can associate with five different β subunits, resulting in αvβ5 which participates in many important cellular processes, including survival and growth factor signaling. Integrin αvβ5 is more widely expressed and is up-regulated after tissue injury. Many different cell types, including muscle cells, express αvβ5 which promotes cell adhesion, migration, and survival. Integrin αv also mediates processes central to immune regulation and inflammation resolution (Ross and Borg, 2001, Albert et al., 1998; Chao et al., 1999; Savill et al., 1990) and manifests phenotypic changes including age-related vision loss accompanied by the accumulation of the retinal pigment epithelium (RPE) lipofuscin and disease (Nandrot et al., 2004).

Irisin was found to communicate with various organs by binding integrins (Park et al., 2020). Integrin αvβ5 was recently identified as a receptor for irisin and plays a significant role in inflammation through its effects on angiogenesis and vascular permeability (Bi et al., 2020b; Lippa et al., 2020). Interactions between integrin αvβ5 and irisin have been reported to upregulate the expression of AMPK which may inhibit cellular apoptosis and inflammation (Bi et al., 2020a, 2020b). While previous studies have demonstrated effects of reduced inflammation, the significance of integrin αvβ5 in the modulation of hemorrhage has yet to be investigated.

Prior research has demonstrated that irisin may have promising therapeutic properties in the management of hemorrhagic shock and its pathologic sequela. This is the first study that examines the effects of inhibition of integrin αvβ5 on hemorrhage-induced pathological disorders. We hypothesize that irisin protects against the damaging sequela of hemorrhagic shock by improving cardiac performance while attenuating the inflammatory response and tissue damages via the integrin receptor.

2. Materials and methods

2.1. Animals and ethics committee approval

CD-1 male mice (25–30 g) were obtained from Charles River Laboratories for conduction of all experiments in this study. All studies were performed under a protocol approved by the Institutional Animal Care and Use Ethics Committee with an approval code: 5008–21, which conforms to the Guide for the Care and Use of Laboratory Animals published by the US National Institutes of Health (NIH Publication No. 85–23, revised 1996).

2.2. Animal and knockdown of integrin β5 by delivery of CRISPR–Gold into the mouse muscle

Animal work was in compliance with National Institutes of Health and the policies of the Animal Care and Use Committee of Rhode Island Hospital. Knockdown of integrin β5 in muscles was performed by using CRISPR/Cas-9 gene editing (1,2). Two-month-old mice were injected with 2 μl of CRISPR–Gold (50pmole of Cas9 and 50pmoles of guide RNAs) with 5 μg of PAsp (DET) in the tibialis anterior muscle (TA). An equal volume of PBS was used as a control. Hemorrhage protocols were performed at 2 weeks following injection.

2.3. Surgical procedure preparation

Mice were anesthetized with 1–4% isoflurane in oxygen and then transferred to the nose cone. The mice were placed on a warming pad and temperature was evaluated by a rectal thermometer. Surgical preparation was performed in the left and right inguinal areas. After local hair shaving, diluted lidocaine (0.5%) was injected under the skin of the anticipated incision. Using sharp scissors, a 2 cm long straight incision was made starting immediately from the medial thigh towards the knee to fully expose the area overlying the femoral artery. The femoral nerve, artery and vein were isolated from the connective tissue using arterial forceps as previous described (Kulthinee et al., 2022). The right and left femoral arteries were inserted with PE-10 fused to PE-50 tubes containing heparinized saline. The right femoral artery catheter was connected to a 1 ml-syringe which would be used for the hemorrhage procedure. The left femoral artery catheter was connected to a pressure transducer to monitoring mean arterial pressure (MAP), which was recorded in Power Lab Data Acquisition (ADInstruments).

2.4. Induction of hemorrhage

Hemorrhage induction was carried out according to the previously established protocol (Kulthinee et al., 2022). In brief, hemorrhage was induced by removing blood from the right femoral artery until MAP reached 35–45 mmHg. The left femoral artery was used for continuous MAP monitoring. If the MAP surpassed 45 mmHg, additional blood was withdrawn from the right femoral artery. If the MAP dropped below 35 mmHg, approximately 0.2 ml of Lactated Ringer's Solution (LRS) was infused into the right femoral artery. The mice were kept at a MAP range of between 35 and 45 mmHg for 60 min.

2.5. Experimental group design

Experimental groups consisted of groups of CD-1 mice in which animals were subjected to hemorrhage and resuscitation. Briefly, at the end of the 60 min of hemorrhage, mice were resuscitated with three times the volume of total blood loss with LRS, using a sterilized syringe over a 15-min period. The resuscitation fluids were infused through the femoral catheter as described in the above procedure. The mice were assigned to one of seven groups as following: I) Sham group received identical surgical operation without induction of hemorrhage ($n = 5$); II) Hemorrhage (Hemo) group underwent hemorrhage and resuscitation as described above in the "induction of hemorrhage" section ($n = 6$); III) Hemo + Irisin group received 0.5 μg/kg of intravenous irisin in LRS ($n = 5$); IV) Hemo + Cilengitide group received 1 mg/kg of intravenous Cilengitide in LRS ($n = 6$); V) Hemo + Irisin + Cilengitide group received 0.5 μg/kg of intravenous irisin and 1 mg/kg of Cilengitide in LRS ($n = 5$); VI) Irisin + RGDS group received 0.5 μg/kg of intravenous irisin and 1 mg/kg of RGDS peptide in LRS ($n = 5$); VII) Hemo + Vehicle group received saline in LRS ($n = 7$).

2.6. Experimental group in integrin β5 knockdown (KD)

The experimental groups were designed to one of following: I) Shamoperated group received identical surgical operation without induction of hemorrhage ($n = 4$); II) Hemo + integrin β5 KD in which integrin β5 KD mice were subjected to 1 h of hemorrhage and a subsequent 2 h of resuscitation as described in the "induction of hemorrhage" section (group $n = 6$); III) Irisin + Hemo + integrin β5 KD groups in which integrin β5 KD mice were subjected 1 h of hemorrhage and a subsequent 2 h of resuscitation and received 0.5 μg/kg of intravenous irisin in LRS ($n = 6$).

2.7. Measurement of cardiac function

Echocardiography was performed with a CX50 system equipped with L15–7io broadband linear array (Philips, Cambridge, MA, USA). Mice were anesthetized with a continuous inhalation of 1–3% isoflurane via nose cone for the duration of the procedure. The mice were placed on a heating pad in the supine position to maintain a body temperature. The hair covering the chest was removed using Nair for 1 min and 30 s. Warm gel was applied, and chest compression was avoided. B mode and M-mode images were acquired in the parasternal short axis of the left ventricle at the level of papillary muscles. EF, FS, and HR were determined. Three to six consecutive cardiac cycles were used to assess the dimensions and heart rate through M-mode. The measurements were made by an experienced operator in a double blinded manner.

2.8. Measurement of cytokines using Enzyme-linked immunoassay (ELISA)

The concentration of IL-6 and TNF-α in serum were measured using a commercially available enzyme-linked immunosorbent assay (ELISA) kit (R & D systems, Minneapolis, MN, USA). Assays were performed following the manufacturer's instructions. Briefly, a 10× diluted serum or 1.5 mg/ml tissue protein along with known concentrations of cytokine standards were applied to the primary antibody pre-coated 96-well ELISA plates. After overnight incubation at 4 °C, a biotinylated secondary antibody was applied and incubated for one hour at room temperature. After incubation, streptavidin-horseradish peroxidase

(SAHRP) solution was applied, followed by tetramethylbenzidine (TMB) substrate solution. Concentrations of the cytokines were estimated from the absorbance at 450 nm using a spectrophotometer (SpectraMax M2e Multi-Mode Microplate Reader, Molecular Device, LLC, San Jose, CA, USA). Protein concentrations in the tissue lysates were quantified using the bicinchoninic acid protein assay kit (Thermo Fisher Scientific, Waltham, MA, USA).

2.9. Hematoxylin and eosin (H&E) staining and assessment of infiltration of inflammatory cells in tissues

Freshly isolated skeletal muscle, heart tissue, and lung were placed in 10% formalin for 24 to 48 h to fix prior to processing. Tissues were sectioned into 5 μm slices. After fixation, the tissues were dehydrated with gradient alcohol and then embedded in paraffin for thin sectioning. Hematoxylin and eosin (H&E) staining was used for evaluation using light microscopy of the alveolar septal thickness in the lungs and inflammatory cells infiltrations in the skeletal muscle and the cardiac tissue samples. The tissues samples were observed under a light microscope, and photomicrographs were taken of approximately 5–10 randomly selected fields of each section for analysis using NIH image J software. Scoring of tissue damage and inflammatory cell infiltration were conducted in a double-blind manner.

2.10. TUNEL staining

For the TUNEL experiment, an ApopTag detection kit was used (ApopTag® In Situ Apoptosis Detection Kits, S7100, Millipore, USA). Tissue sections were deparaffined and rehydrated for 10 min and then digested with proteinase K (Thermo Fisher Scientific, #EO0491) for 15 min and quenched with 3% hydrogen peroxide to prevent peroxidase activity. The slides were then washed in PBS for 5 min and reacted with equilibrium buffer for 2 min. The terminal deoxynucleotidyl transferase (TdT) enzyme was then added onto the slides and incubated in a humidified chamber for 1 h. Anti-digoxigenin conjugate were then dropped onto the slides and incubated in a humidified chamber for 1 h. After washing the slides with PBS, peroxidase substrate solution was added to the slide for 30 min for staining. The slides were washed with distilled H_2O and counterstained with 0.5% methyl green for 10 min at room temperature. The slides were then dehydrated with N-butanol and xylene and mounted with Permount. Negative control was performed without active TdT. Apoptosis was quantified by counting the numbers of apo-positive nuclei in each slide. Independent counting was performed by a blinded investigator.

2.11. Immunofluorescent staining

The slides were deparaffinized and antigen was retrieved through citraconic buffer boiling for 45 min. The blocking step was performed using 1% BSA for 30 min at room temperature. After blocking, the slide sections were incubated with anti-mouse integrin αvβ5 (Abcam) and anti mouse α sarcomeric actin IgM (Millipore-Sigma) (1:200) overnight at 4 °C. Sections were then washed 3 times in phosphate buffer saline (PBS) before being incubated with the corresponding secondary antibodies labeled with Alexa Fluor555 or FITC (Thermo Fisher Scientific) at 1:200 for one hour in dark and humidified conditions. The slides were washed three additional times with PBS. Slides were then mounted with DABCO (Millipore-Sigma) and sealed with oil. The immunofluorescent images were captured through a laser scanning microscope.

2.12. Western blotting

Protein levels from skeletal muscle were measured by western blotting using tissue lysates (50 μg/lane) as described in our previous methods (Yano et al., 2020). In brief, the blots were incubated with their respective polyclonal antibodies, which included polyclonal rabbit Beta-actin (Cell signaling Technology, Beverly, MA), integrin αvβ5 (Abcam), phosphorylated AMPK, and non-phosphorylated AMPK (Cell signaling Technology, Beverly, MA) at a diluted concentration of 1:1000. The signals were then visualized using anti-rabbit horseradish peroxidase-conjugated secondary antibody (1:2000). The results were visualized with Super Signal West Pico ECL chemiluminescence reagent (Thermo-Fisher Scientific). Densitometric analysis for the blots were completed using NIH Image J processing program.

2.13. ELISA analysis of integrin αv and irisin binding in vitro

Stable cell line for over-expression of integrin αv was established by transfection of embryonic stem cell ($Nkx2.5^{+}$ cells) with integrin αv vector (Sino Biological). Stable transfections of integrin αv vector and control vectors were carried out using Lipofectamine 2000 Transfection Reagent (Invitrogen) following the manufacturer's instructions. Individual cells were isolated and selected with G418. The binding of irisin with integrin αv was identified using ELISA (abcam). Irisin antibody was also included to antagonize the binding of irisin with integrin αv.

2.14. Production of sgRNA of integrin β5

In vitro T7 transcription of sgRNA for integrin β5 was carried out. Briefly, the DNA templates for in vitro transcription of integrin β5 sgRNAs was prepared using PCR. The sequence of guide RNAs was used for integrin β-*5* knockdown experiments. A single sequence for sgRNAs was identified for targeting integrin β-*5* knockdown was used; Integrin b5 gRNA 1.1 CACCGACCGAGAGGTGATGGACCGT; Integrin b5 gRNA 1.2 AAACACGGTCCATCACCTCTCGGTC. PCR amplification was performed using Polymerase following the manufacturer's protocol. In vitro transcription of RNA was carried out using the MEGAscript T7 kit (AMB13345, Thermo Fisher Scientific), and purification of the resulting RNA was performed using the MEGAclear kit according to the manufacturer's protocol. The transcribed sgRNAs was eluted into 20 mM HEPES buffer. The concentration of RNAs was measured using a Nanodrop 2000 spectrophotometer, and the final sg RNAs were stored at −80 °C for experiments.

2.15. Delivery system for sgRNA-CRISPR–Gold synthesis

The synthesis of CRISPR–Gold conjugation was utilized as a delivery vehicle of sgRNA and was carried out according to the protocol as described previously (3–6). GNPs (60 nm in diameter, 450 nM, TED PELLA) were reacted with a 5′ thiol-modified single stranded oligonucleotide (DNA-SH), 26 bases in length (/5ThioMC6-D/GAAATATGCCAGAAATATCTGTCAGA, 200 μM, Integrated DNA Technologies IDT). The reaction was carried out in nuclease-free water in a 160 μl tube. Sodium citrate buffer (100 mM, pH 3.5, 40 μl) was added to the reaction. Unconjugated DNA-SH was then removed by centrifugation at 3000 ×*g* for 10 min and was washed twice with 20 mM

HEPES buffer. The GNP–DNA solution was stored at 4 °C. CRISPR–Gold was synthesized using a layer-by-layer method. Cas9 (50pmole in 10 μl) and sg RNAs (50pmole in 10 μl) were mixed in 80 μl of Cas9 buffer (50 mM HEPES (pH 7.5), 300 mM NaCl, and 10% (vol./vol.) glycerol for 5 min at room temperature. The reaction solution was then added to the GNP–DNA solution (0.45pmole of GNPs), which generated GNP–Cas9. Sodium silicate (6 mM, 2 μl) was added to the GNP–Cas9 RNP solution, which was followed by incubation for 5 min at room temperature. Unbound molecules were removed by centrifuging the mixture using an EMD Millipore Amicon Ultra-4 30 kDa at 2000 ×*g* for 5 min. GNP–Cas9 RNP–silicate was recovered and mixed with 5 μg of PAsp (DET) (NOFAmerica corporation) solution and then incubated for 5 min at room temperature to form the last layer of CRISPR–Gold immediately prior to treatment.

2.16. Characterization of Gold-CRISPR-sgRNA

Dynamic light scattering (DLS) and zeta potential assessment were carried out. Measurements of the zeta potential were made with a Zetasizer Nano ZS instrument (Malvern Instruments) to examine the stability. Size distribution was also analyzed with DLS.

2.17. In vitro knockdown of integrin β5

The in vitro cell experiments were carried out according to the methods described previously (3, 7). Briefly, cells (1 ml volume) were treated with 0.45 pmol GNP–Donor, 8 μg Cas9, 2 μg gRNA, 2 μl (6 mM) sodium silicate, and 10 μg PAsp (DET). Cas9 and gRNA solution were mixed with Cas9 buffer (50 mM HEPES (pH 7.5), NaCl (300 mM) and 10% (vol/vol) glycerol) and then added to the GNP–Donor solution. Freshly diluted sodium silicate (6 mM; 2 μl) was added to the GNP solution. The recovered GNPs were resuspended in 20 mM HEPES buffer (100 μl), which was followed by adding PAsp (DET) polymer to generate a final concentration of 100 μg/ml. The CRISPR–Gold solution was added to cells to produce a final Cas9 concentration of 8 μg/ml of Cas9. The cells were incubated with CRISPR–Gold in serum-free Opti-MEM for 6 4 h prior to changing to fresh culture media (DMEM). Short hairpin RNA (shRNA) against mouse integrin receptor (IR) (Santa Cruz Biotechnology) was used as the control of knockdown.

2.18. Quantitative real-time PCR

RNA was isolated from skeletal muscle tissues of euthanized mice using TRIzol (Invitrogen) following manufacturer's instructions. cDNA was synthesized using BioRad iScript Reverse Transcription Supermix. qPCR was conducted using Applied Biosystems TaqMan probes for integrin receptor (F Primer; R Primer:). Integrin β-*5*-*F*: TCCAACTGTGACAATGGAGTG; Integrin β-*5*-R: GCTCTGAGCTCAATCAAGCC. Experiments were conducted on a StepOne Real-Time PCR System (Life Technologies) and analyzed using the delta–delta Ct method.

2.19. Statistical analysis

The data are presented as means ± SE. Data were analyzed by one-way ANOVA, with the Bonferroni correction for multigroup comparisons. Statistical analysis was performed

by Graphpad Prism 9 software (GraphPad Software, San Diego, CA). Significance was established at a p value <0.05.

3. Results

3.1. Inhibition of integrin αvβ5 suppressed the effects of irisin on hemodynamic

Hemorrhage and resuscitation were performed, as shown in Fig. 1A. Hemorrhage resulted in the reduction of integrin αvβ5 (Fig. 1B&C). To define a direct interaction of integrin αvβ5 and irisin, we used immunoprecipitation to identify the interaction between integrin αvβ5 and irisin in vitro. We extended our study to determine whether over-expression of integrin αvβ5 could lead to an increase in the binding of irisin by including an *invitro* experiment in which mouse embryonic stem cell line ($Nkx2.5^+$ cells) over-expressed integrin αvβ5 (Fig. 2A). We found that the over-expression of integrin αvβ5 resulted in a significant binding increase in irisin by ELISA analysis in Fig. 2B. Interestingly, binding was inhibited by the integrin αvβ5 antibody, and demonstrated that irisin binds specifically to the integrin αvβ5, indicating a direct interaction of integrin αvβ5 and irisin.

As shown in Fig. 3 A, illustrating the time course during hemorrhage and resuscitation, inhibition of integrin αvβ5 by cilengitide in the Hemo + Cilengitide group and Hemo + Irisin + Cilengitide manifests lower MAP after resuscitation when compared to the irisin-treated (Hemo + Irisin) group (Fig. 3B). The MAP in the Irisin treated hemorrhage group restored to near baseline value. There was no difference in MAP prior to hemorrhage between different groups (Fig. 3C). Hemorrhage resulted in the depression in MAP at 20 min of resuscitation, which was rescued by the infusion of irisin. Irisin-induced improvement in MAP was mitigated by co-infusion with Cilengitide (Fig. 3D).

Additionally, we used CRISPR/Cas9-sgRNA system to knockdown integrin β5, a subunit of integrin αvβ5 to examine the effect of integrin β5 knockdown on hemorrhage, which is shown in Fig. 4A–D. A reduction of integrin β5 was shown after delivery of CRISPR-sgRNA integrin β5 in the cultured cells (Fig. 4E&F). In vivo delivery of Gold-CRISPR-sgRNA integrin β5 resulted in suppression of integrin β5 mRNA (Fig. 4G, H and I) and did not have systemic effects on body growth (Fig. 4J). As shown in Fig. 5A–C, knockdown of integrin β5 manifests a decline in the MAP after hemorrhage as compared to the sham group, but there is no difference in the MAP between the Hemo + integrin β5 knockdown and Hemo + integrin β5-KD treated with Irisin. This implies that the protective effects of irisin are impaired when integrin β5 is inhibited.

3.2. Inhibition of integrin αvβ5 suppressed the effects of irisin on cardiac function

To compare the cardiac function between the sham and hemorrhage groups, mice were evaluated using echocardiography. As shown in Fig. 6A and B, ejection fraction (EF) and fractional shortening (FS) were significantly reduced in the hemorrhage groups compared to the sham groups. Irisin treatment significantly improved both EF and FS in the hemorrhage group compared to the vehicle treatment group. However, the improvement in EF and FS by irisin treatment was blocked by co-infusion of cilengitide. There were no statistically significant differences in the left ventricular dimensions and wall thicknesses, including LV

internal dimensions (LVID), posterior wall thicknesses (PW) during systole and diastole (LVIDd, LVIDs, LVPWd, LVPWs), left ventricular volume, and heart rate (HR) (Fig. 6C–J) between drug treatments. Likewise, there was no improvement in cardiac performance in mice exposed to hemorrhage by the knockdown of integrin β5 even after irisin treatment (Fig. 7A–J). The results indicate that the inhibition of integrin αvβ5 by Cilengitide or CRISPR/Cas 9-sgRNA diminished the improvement of cardiac performance induced by irisin in hemorrhage.

3.3. Inhibition of integrin αvβ5 mitigated the effects of irisin on alleviated histological damage in myocardium, skeletal muscle, and lung tissues

Analyses with hematoxylin and eosin (H&E) staining were performed to evaluate the histological changes in skeletal muscles, myocardium, and lung induced by hemorrhage. Hemorrhage resulted in more severe inflammatory cell infiltrations in myocardium and skeletal muscles when compared to that in the sham group and irisin-treated group. Inhibition of integrin αvβ5 decreased the effects of irisin on alleviated inflammatory cell infiltrations ($p < 0.0001$), as shown in Fig. 8A–D. Lung tissues showed significant thickening of the alveolar septal wall observed in the hemorrhage group compared to the sham group. Irisin treatment significantly reduced the degree of alveolar wall thickening ($p < 0.0001$) (Fig. 8E & F), which was abrogated by inhibition of integrin αvβ5. Furthermore, as shown in Fig. 9A–D, irisin did not show any improvement in inflammatory cell infiltrations in myocardium and skeletal muscles in mice with knockdown of integrin β5. Additionally, in mice with knockdown of integrin αvβ5, alveolar septal wall thickness did not improve in the irisin treatment group (Fig. 9E&F $p < 0.0001$).

3.4. Inhibition of integrin αvβ5 increased release of inflammatory cytokines in hemorrhage

Hemorrhage promotes an inflammatory response that exacerbates pathological adverse outcomes. To assess the effect of hemorrhagic shock on the inflammatory response, IL-6 and TNF-α in serum were measured. As seen in Fig. 10A & B, following two hours of resuscitation, the serum level of IL-6 and TNF-α increased markedly in the hemorrhagic group and the elevations of cytokine levels were reversed with irisin treatment. In addition, the knockdown of integrin β5 did not show the effects of irisin in attenuating the release of IL6 in mice exposed to hemorrhage as shown in Fig. 10C. This suggests that inhibition of integrin αvβ5 attenuated the inhibitory effect of irisin on decreased levels of IL-6 and TNF-α in serum when induced by hemorrhage.

3.5. Inhibition of integrin αvβ5 diminished the effect of irisin in reduction of apoptosis in tissues

We performed TUNEL staining in myocardium, skeletal tissues, and lung tissues to evaluate the degree of apoptosis. As shown in Fig. 11A &B, almost no TUNEL positive cells were observed in the sham operated group while TUNEL positive cells were observed in the myocardium of the hemorrhage and vehicle treated groups. Irisin treatment demonstrated significantly reduced numbers of TUNEL positive signal. Likewise, irisin treatment attenuated TUNEL positive staining in skeletal muscles (Fig. 11C&D) and lung tissues (Fig. 11E–F). However, the effects of the reduced apoptotic signals by irisin were mitigated

by the pharmacologic inhibition of integrin αvβ5 with Cilengitide. In addition, irisin did not show the effect of reducing apoptosis in the myocardium (Fig. 12A&B), skeletal muscles (Fig. 12C&D) and lung tissues (Fig. 12E&F) following knockdown of the integrin β5.

3.6. Inhibition of integrin αvβ5 diminished irisin-induced phosphorylation of AMPK

As shown in Fig. 13, western blot revealed reduced levels of p-AMPK in skeletal muscles of the hemorrhage group compared to the sham operated group. After the treatment with irisin, the level of p-AMPK increased in skeletal muscles (Fig. 13A&B), but only slightly in the myocardium (Fig. 13C&D). However, enhanced p-AMPK by irisin was reduced by Cilengitide treatment in the skeletal muscles and the myocardium. Likewise, as shown in Fig. 13, inhibition of integrin β5 with integrin β5 sgRNA did not shown an increase in phosphorylated AMPK by irisin in both skeletal muscles and the myocardium in mice exposed to hemorrhage (Fig. 13E&F and Fig. 13G&H).

4. Discussion

4.1. Salient findings

In this study, we have demonstrated that integrin αvβ5 contributes significantly to modulating pathological disorders in mice exposed to hemorrhage. Our studies showed that blocking integrin αvβ5 with Cilengitide diminished the protective effect induced by irisin. Irisin treatment resulted in improvements in cardiac performance and hemodynamics while blunting the inflammatory response and apoptotic signals in the myocardium, skeletal muscles, and lung tissue following hemorrhage, which was diminished when the integrin αvβ5 was pharmacologically blocked, indicting the critical role of integrin αvβ5 in modulating the function of irisin during hemorrhage. Furthermore, we demonstrated that knockdown of the β5 integrin eliminated the protective effect induced by irisin against hemorrhage, confirming the paramount role that integrin αvβ5 plays in irisin's functioning. Taken together, our novel findings establish that integrin αvβ5 primarily interacts with irisin to exert cardioprotective, anti-inflammatory, and anti-apoptotic effects during hemorrhage.

4.2. Role of integrin αvβ5/irisin in modulating cardiac function in hemorrhage

Wang et al. (2018) previously demonstrated that the treatment of rats with irisin resulted in improved ventricular function through reduced apoptosis and preserved mitochondrial functioning in ischemia/reperfusion injury (Wang et al., 2018). It has also been shown that heart failure is associated with reduced levels of serum irisin (Abd El-Mottaleb et al., 2019). We have found that integrin αvβ5 is abundantly expressed in the skeletal muscles, which is reduced in response to hemorrhage. We also found that irisin treatment was associated with improved cardiac performance parameters. These improvements were negated by blocking integrin αvβ5 with Cilengitide or through CRISPR-gene editing to knock down the integrin αvβ5 receptor, implying that integrin αvβ5 was responsible for irisin-induced cardiac performance in hemorrhage. It was reported that integrin αvβ5 was expressed in cardiomyoblasts, vascular endothelial cells, and cardiomyocytes, which mediates cardiac function and development (Sarrazy et al., 2014; Chen et al., 2016; Israeli-Rosenberg et al., 2014; Noutsias et al., 2001). It remains to be determined whether the change in cardiac performance following the inhibition of integrin αvβ5 results from the

effect of cardiomyocytes or non-cardiomyocytes in hemorrhage, which needs verification in future studies. Additionally, enhancement of proinflammatory factors such as TNF-α release following integrin αvβ5 inhibition could contribute to depressed cardiac functioning in hemorrhage.

It has been shown that Cilengitide increases the deposition of fibrillar collagen in the myocardium, revealing that inhibition of integrin αvβ5 signaling mediates systemic fibrosis in systemic sclerosis (Bagnato et al., 2018). It was also reported that inhibition of integrin αvβ5 causes a cardioprotective effect by suppressing doxorubicin-induced cardiac fibrosis (Sui and Hou, 2021). Conversely, it has been observed that stimulation of integrin αvβ5 contributed to irisin-induced cardiac protection (Lin et al., 2021). Irisin has been shown to interact with integrin αvβ5 receptor in vascular cells to manifest protective effects (Bi et al., 2020a; Roggia and Ueta, 2015). This may indicate that inhibition of integrin αvβ5 in the vascular cells supporting the myocardium contributes to the depression of cardiac function. Irisin may also cause its physiologic function via unidentified irisin receptors or non-receptors binding pathway (Fu et al., 2021). Our results indicated that irisin induced a slight increase in phosphorylated AMPK in hemorrhage, which was blocked by the inhibition of the integrin αvβ5, indicating that AMPK may be involved in the function of irisin/integrin αvβ5 pathway in hemorrhage.

4.3. Role of integrin αvβ5/irisin in modulating inflammatory processes in hemorrhage

We demonstrated that the levels of inflammatory cytokines increased significantly after blocking integrin αvβ5 with Cilengitide, or by gene-knockdown, revealing that the integrin αvβ5 is necessary for blunting the inflammatory response following hemorrhage. Previous studies have shown that irisin tempers the inflammatory cascade by reducing the production of pro-inflammatory cytokines in association with (M2) macrophage polarization, and blocking the formation of inflammasomes (Dong et al., 2016; Li et al., 2021b; Ostrowski et al., 2000; Xiong et al., 2018). This is consistent with our findings that irisin decreases the production of systemic inflammatory factors. Irisin post-treatment has been shown to increase expression of integrin αvβ5, which was associated with decreased IL-1β and TNF-α levels in intracerebral hemorrhage (Wang et al., 2022), which supports that integrin αvβ5 is critical to the function of irisin in alleviating pathological disorders (Park et al., 2020). Knockdown of integrin αvβ5 by siRNA, or Cilengitide, has been shown to suppress PPARγ-induced M2 marker genes (Yao et al., 2018). Mice lacking αvβ5 on hematopoietic cells have illustrated enhanced susceptibility to chemical colitis, suggesting the important role of integrin αvβ5 for tissue repair (Kumawat et al., 2018). In addition, the αvβ5 integrin exhibits latent stimulatory effects on IL-8 secretion by fibronectin (Lowrie et al., 2004). In our studies, in addition to finding that inhibition of integrin αvβ5 resulted in a remarkable increase in systemic proinflammatory factor, we also found an increase in the infiltration of inflammatory cells in the tissues, which likely results from neutrophils, macrophages, leukocytes, and other immune cells responding to tissue injury (Ju et al., 2021). It will be interesting to define which specific population of inflammatory cells contributes to the infiltration of inflammatory cells in the tissues in response to hemorrhage following the inhibition of integrin αvβ5.

4.4. Role of integrin αvβ5/irisin in modulating muscles in hemorrhage

It has been shown that a downregulation of integrin αvβ5 in vascular smooth muscle cells (VSMCs) is considered a potential factor for reduced cell motility following vascular injury (Witzenbichler et al., 1999). Irisin was reported to inhibit nicotine-mediated macrophage infiltration and smooth muscle cell proliferation in atherosclerosis, but the protection induced by irisin was abrogated by the administration of Cilengitide, suggesting the involvement of integrin αvβ5 in developing protective effects in atherosclerosis (Li et al., 2021a). The inhibition of integrin αvβ5 reduces allergen-induced increases in airway smooth muscle thickness in two models of asthma, demonstrating that integrin promotes anti-inflammatory pathways in smooth muscles (Wolf et al., 2011). In agreement with our observation, another study revealed that inhibition of integrin αvβ5 attenuated the protective effect of collagen-type-IV-α-2-chain on cell viability in cardiomyoblasts under hypoxic condition via increased phosphorylation of FAK and Akt (Kanazawa et al., 2017). Our findings revealed that knockdown of integrin αvβ5 in skeletal muscles exacerbated cardiac depression in response to hemorrhage, which may be related to circulating cytokine changes following knockdown of muscle integrin αvβ5. Cross-talk exists between either skeletal muscles and the myocardium or between other organs contributing to the modulation of cardiac performance (Call et al., 2015; Xu et al., 2023), which also supports our finding of the protective effects of integrin αvβ5 in skeletal muscles and cardiac performance in response to hemorrhage.

4.5. Role of integrin αvβ5 and irisin in modulating apoptosis and survival in hemorrhage

Irisin treatment provides protection against neuronal apoptosis following subarachnoid hemorrhage by interacting with integrin αvβ5 and reducing pro-inflammatory stimuli (Tu et al., 2021; Wang et al., 2022). Integrin αvβ5 was reported to reduce inflammation through its effects on angiogenesis and vascular permeability in addition to reduced apoptosis (Bi et al., 2020b; Lippa et al., 2020). Tumor necrosis factor-related apoptosis is associated with activation of integrin αvβ5 receptor in lung cancer cells (Cho et al., 2016). The classic integrin receptors binding integrin αvβ5 could mediate protection of topoisomerase (Topo)-induced apoptosis (Uhm et al., 1999), which is in agreement with a report that blockade of integrin αvβ5 inhibited survival, therefore promoting activity in ovarian cancer cells (Lane et al., 2010), induced apoptosis in human umbilical endothelial cells (HUVECs) (Maubant et al., 2006) and cell lines U87 MG and DAOY (Taga et al., 2002). However, intravitreal injection of anti-integrin αvβ5 antibody in vivo also inhibited astrocyte loss in early diabetic retinopathy (Yun et al., 2016). The protective effects of blocking integrin αvβ5 in modulating apoptosis is likely related to various models and doses of integrin αvβ5 inhibitors.

5. In conclusion

Our results indicate that irisin treatment of mice following hemorrhage and resuscitation improves cardiovascular function, reduces inflammation and apoptosis, and prevents tissue injury. These protective properties rely on the interaction between irisin and integrin αvβ5. Our study offers findings that may signify new treatment modalities for hemorrhagic shock and secondary outcomes following treatment.

Acknowledgments

The work is supported by the National Institute of General Medical Sciences (R01GM 141339), United States; the National Heart, Lung, and Blood Institute Grants (R01 HL089405), United States.

Data availability

Data will be made available on request.

References

Abd El-Mottaleb NA, Galal HM, El Maghraby KM, Gadallah AI, 2019. Serum irisin level in myocardial infarction patients with or without heart failure. Can. J. Physiol. Pharmacol 97 (10), 932–938. 10.1139/cjpp-2018-0736. [PubMed: 30958967]

Albert ML, Pearce SF, Francisco LM, Sauter B, Roy P, Silverstein RL, Bhardwaj N, 1998. Immature dendritic cells phagocytose apoptotic cells via alphavbeta5 and CD36, and cross-present antigens to cytotoxic T lymphocytes. J. Exp. Med 188 (7), 1359–1368. 10.1084/jem.188.7.1359. [PubMed: 9763615]

Bagnato GL, Irrera N, Pizzino G, Santoro D, Roberts WN, Bagnato G, Bitto A, 2018. Dual αvβ3 and αvβ5 blockade attenuates fibrotic and vascular alterations in a murine model of systemic sclerosis. Clin. Sci. (Lond.) 132 (2), 231–242. 10.1042/CS20171426. [PubMed: 29237724]

Bi J, Zhang J, Ren Y, Du Z, Li T, Wang T, Wu R, 2020a. Irisin reverses intestinal epithelial barrier dysfunction during intestinal injury via binding to the integrin αVβ5 receptor. J. Cell. Mol. Med 24 (1), 996–1009. 10.1111/jcmm.14811. [PubMed: 31701659]

Bi JB, Zhang J, Ren YF, Du ZQ, Zhang YY, Liu C, Wu RQ, 2020b. Exercise hormone irisin mitigates endothelial barrier dysfunction and microvascular leakage-related diseases. JCI Insight 5 (13). 10.1172/jci.insight.136277. Article e136277. [PubMed: 32516137]

Bilski J, Mazur-Bialy AI, Brzozowski B, Magierowski M, Jasnos K, Krzysiek-Maczka G, Brzozowski T, 2015. Moderate exercise training attenuates the severity of experimental rodent colitis: the importance of crosstalk between adipose tissue and skeletal muscles. Mediat. Inflamm 2015 10.1155/2015/605071. Article 605071.

Boström P, Wu J, Jedrychowski MP, Korde A, Ye L, Lo JC, Spiegelman BM, 2012. A PGC1-α-dependent myokine that drives brown-fat-like development of white fat and thermogenesis. Nature 481 (7382), 463–468. 10.1038/nature10777. [PubMed: 22237023]

Call JA, Chain KH, Martin KS, Lira VA, Okutsu M, Zhang M, Yan Z, 2015. Enhanced skeletal muscle expression of extracellular superoxide dismutase mitigates streptozotocin-induced diabetic cardiomyopathy by reducing oxidative stress and aberrant cell signaling. Circ. Heart Fail 8 (1), 188–197. 10.1161/CIRCHEARTFAILURE.114.001540. [PubMed: 25504759]

Chao D, Bahl P, Houlbrook S, Hoy L, Harris A, Austyn JM, 1999. Human cultured dendritic cells show differential sensitivity to chemotherapy agents as assessed by the MTS assay. Br. J. Cancer 81 (8), 1280–1284. 10.1038/sj.bjc.6694366. [PubMed: 10604723]

Chatpun S, Cabrales P, 2011. Cardiac systolic function recovery after hemorrhage determines survivability during shock. J. Trauma 70 (4), 787–793. 10.1097/TA.0b013e3181e7954f. [PubMed: 20805773]

Chen C, Li R, Ross RS, Manso AM, 2016. Integrins and integrin-related proteins in cardiac fibrosis. J. Mol. Cell. Cardiol 93, 162–174. 10.1016/j.yjmcc.2015.11.010. [PubMed: 26562414]

Cho C, Horzempa C, Jones D, McKeown-Longo PJ, 2016. The fibronectin III-1 domain activates a PI3-kinase/Akt signaling pathway leading to αvβ5 integrin activation and TRAIL resistance in human lung cancer cells. BMC Cancer 16, 574. 10.1186/s12885-016-2621-6. [PubMed: 27484721]

Dong J, Dong Y, Chen F, Mitch WE, Zhang L, 2016. Inhibition of myostatin in mice improves insulin sensitivity via irisin-mediated cross talk between muscle and adipose tissues. Int. J. Obes 40 (3), 434–442. 10.1038/ijo.2015.200.

Elansary NN, Stonko DP, Treffalls RN, Abdou H, Madurska MJ, Morrison JJ, 2022. Class of hemorrhagic shock is associated with progressive diastolic coronary flow reversal and diminished left ventricular function. Front. Physiol 13, 1033784. 10.3389/fphys.2022.1033784. [PubMed: 36589436]

Erickson HP, 2013. Irisin and FNDC5 in retrospect: an exercise hormone or a transmembrane receptor? Adipocyte 2 (4), 289–293. 10.4161/adip.26082. [PubMed: 24052909]

Fu J, Li F, Tang Y, Cai L, Zeng C, Yang Y, Yang J, 2021. The emerging role of irisin in cardiovascular diseases. J. Am. Heart Assoc 10 (20), e022453 10.1161/JAHA.121.022453. [PubMed: 34622672]

Gaggini M, Cabiati M, Del Turco S, Navarra T, De Simone P, Filipponi F, Basta G, 2017. Increased FNDC5/Irisin expression in human hepatocellular carcinoma. Peptides 88, 62–66. 10.1016/j.peptides.2016.12.014. [PubMed: 28012856]

Hierholzer C, Kalff JC, Omert L, Tsukada K, Loeffert JE, Watkins SC, Tweardy DJ, 1998. Interleukin-6 production in hemorrhagic shock is accompanied by neutrophil recruitment and lung injury. Am. J. Phys 275 (3), L611–L621. 10.1152/ajplung.1998.275.3.L611.

Huh JY, Mougios V, Kabasakalis A, Fatouros I, Siopi A, Douroudos II, Mantzoros CS, 2014. Exercise-induced irisin secretion is independent of age or fitness level and increased irisin may directly modulate muscle metabolism through AMPK activation. J. Clin. Endocrinol. Metab 99 (11), E2154–E2161. 10.1210/jc.2014-1437. [PubMed: 25119310]

Hynes RO, 2002. Integrins: bidirectional, allosteric signaling machines. Cell 110 (6), 673–687. 10.1016/s0092-8674(02)00971-6. [PubMed: 12297042]

Israeli-Rosenberg S, Manso AM, Okada H, Ross RS, 2014. Integrins and integrin-associated proteins in the cardiac myocyte. Circ. Res 114 (3), 572–586. 10.1161/CIRCRESAHA.114.301275. [PubMed: 24481847]

Ju JY, Stelow EB, Courville EL, 2021. Normal gastrointestinal tract inflammatory cells and review of select benign hematolymphoid proliferations. Semin. Diagn. Pathol 38 (4), 6–13. 10.1053/j.semdp.2021.02.001. [PubMed: 33726961]

Kanazawa H, Imoto K, Okada M, Yamawaki H, 2017. Canstatin inhibits hypoxia-induced apoptosis through activation of integrin/focal adhesion kinase/Akt signaling pathway in H9c2 cardiomyoblasts. PLoS One 12 (2), e0173051 (PMID: 28235037). [PubMed: 28235037]

Kim JY, van de Wall E, Laplante M, Azzara A, Trujillo ME, Hofmann SM, Scherer PE, 2007. Obesity-associated improvements in metabolic profile through expansion of adipose tissue. J. Clin. Invest 117 (9), 2621–2637. 10.1172/JCI31021. [PubMed: 17717599]

Koyama S, Aibiki M, Kanai K, Fujita T, Miyakawa K, 1988. Role of central nervous system in renal nerve activity during prolonged hemorrhagic shock in dogs. Am. J. Phys 254 (5 Pt 2), R761–R769. 10.1152/ajpregu.1988.254.5.R761.

Krausz MM, 2006. Initial resuscitation of hemorrhagic shock. World J. Emerg. Surg 1, 14. 10.1186/1749-7922-1-14. [PubMed: 16759354]

Kulthinee S, Wang L, Yano N, Dubielecka PM, Zhang LX, Zhuang S, Zhao TC, 2022. Irisin preserves cardiac performance and insulin sensitivity in response to hemorrhage. Pharmaceuticals (Basel) 15 (10). 10.3390/ph15101193.

Kumawat AK, Yu C, Mann EA, Schridde A, Finnemann SC, Mowat AM, 2018. Expression and characterization of αvβ5 integrin on intestinal macrophages. Eur. J. Immunol 48 (7), 1181–1187. 10.1002/eji.201747318. [PubMed: 29676784]

Kvarstein G, Mirtaheri P, Tønnessen TI, 2003. Detection of organ ischemia during hemorrhagic shock. Acta Anaesthesiol. Scand 47 (6), 675–686. 10.1034/j.1399-6576.2003.00134.x. [PubMed: 12803584]

Lacy-Hulbert A, Smith AM, Tissire H, Barry M, Crowley D, Bronson RT, Hynes RO, 2007. Ulcerative colitis and autoimmunity induced by loss of myeloid alphav integrins. Proc. Natl. Acad. Sci. U. S. A 104 (40), 15823–15828. 10.1073/pnas.0707421104. [PubMed: 17895374]

Lane D, Goncharenko-Khaider N, Rancourt C, Piché A, 2010. Ovarian cancer ascites protects from TRAIL-induced cell death through alphavbeta5 integrin-mediated focal adhesion kinase and Akt activation. Oncogene 29 (24), 3519–3531. 10.1038/onc.2010.107. [PubMed: 20400979]

Li K, Chen J, Wang C, Shao J, Lai Z, Yu X, Liu B, 2021a. Irisin ameliorates nicotine-mediated atherosclerosis via inhibition of the PI3K pathway. Ann. Transl. Med. 9 (9), 805. 10.21037/atm-21-2072.

Li HZ, Qin SG, Liang QQ, Xi Y, Bo WY, Cai MX, Tian Z, 2021b. Exercise training enhances myocardial mitophagy and improves cardiac function via Irisin/FNDC5-PINK1/Parkin pathway in MI mice. Biomedicines 9 (6). 10.3390/biomedicines9060701. Article 701.

Li Q, Zhang MM, Zhao Y, Dong ML, 2021c. Irisin protects against LPS-stressed cardiac damage through inhibiting inflammation, apoptosis, and pyroptosis. Shock 56 (6), 1009–1018. 10.1097/shk.0000000000001775.

Lin C, Guo Y, Xia Y, Li C, Xu X, Qi T, Tao L, 2021. FNDC5/Irisin attenuates diabetic cardiomyopathy in a type 2 diabetes mouse model by activation of integrin αV/β5-AKT signaling and reduction of oxidative/nitrosative stress. J. Mol. Cell. Cardiol 160, 27–41. 10.1016/j.yjmcc.2021.06.013. [PubMed: 34224725]

Lippa RA, Barrett J, Pal S, Rowedder JE, Murphy JA, Barrett TN, 2020. Discovery of the first potent and selective α. Eur. J. Med. Chem 208, 112719 10.1016/j.ejmech.2020.112719. [PubMed: 32865176]

Lowrie AG, Salter DM, Ross JA, 2004. Latent effects of fibronectin, alpha5beta1 integrin, alphaVbeta5 integrin and the cytoskeleton regulate pancreatic carcinoma cell IL-8 secretion. Br. J. Cancer 91 (7), 1327–1334. 10.1038/sj.bjc.6602132. [PubMed: 15354211]

Matsuo Y, Gleitsmann K, Mangner N, Werner S, Fischer T, Bowen TS, Adams V, 2015. Fibronectin type III domain containing 5 expression in skeletal muscle in chronic heart failure-relevance of inflammatory cytokines. J. Cachexia. Sarcopenia Muscle 6 (1), 62–72. 10.1002/jcsm.12006. [PubMed: 26136413]

Maubant S, Saint-Dizier D, Boutillon M, Perron-Sierra F, Casara PJ, Hickman JA, Van Obberghen-Schilling E, 2006. Blockade of alpha v beta3 and alpha v beta5 integrins by RGD mimetics induces anoikis and not integrin-mediated death in human endothelial cells. Blood 108 (9), 3035–3044. 10.1182/blood-2006-05-023580. [PubMed: 16835373]

Nandrot EF, Kim Y, Brodie SE, Huang X, Sheppard D, Finnemann SC, 2004. Loss of synchronized retinal phagocytosis and age-related blindness in mice lacking alphavbeta5 integrin. J. Exp. Med 200 (12), 1539–1545. 10.1084/jem.20041447. [PubMed: 15596525]

Noutsias M, Fechner H, de Jonge H, Wang X, Dekkers D, Houtsmuller AB, Poller W, 2001. Human coxsackie-adenovirus receptor is colocalized with integrins alpha(v)beta(3) and alpha(v)beta(5) on the cardiomyocyte sarcolemma and upregulated in dilated cardiomyopathy: implications for cardiotropic viral infections. Circulation. 104 (3), 275–280. 10.1161/01.CIR.104.3.275. [PubMed: 11457744]

Ostrowski K, Schjerling P, Pedersen BK, 2000. Physical activity and plasma interleukin-6 in humans – effect of intensity of exercise. Eur. J. Appl. Physiol 83 (6), 512–515. 10.1007/s004210000312.

Ouyang HC, Li Q, Zhong JK, Xia FF, Zheng SL, Lu JH, Hu YZ, 2020. Combination of melatonin and irisin ameliorates lipopolysaccharide-induced cardiac dysfunction through suppressing the Mst1-JNK pathways. J. Cell. Physiol 235 (10), 6647–6659. 10.1002/jcp.29561. [PubMed: 31976559]

Pan JA, Zhang H, Yu Q, Zhang JF, Wang CQ, Gu J, Chen K, 2021. Association of circulating irisin levels and the characteristics and prognosis of coronary artery disease. Am J Med Sci 362 (1), 63–71. 10.1016/j.amjms.2021.02.020. [PubMed: 33647285]

Park EJ, Myint PK, Ito A, Appiah MG, Darkwah S, Kawamoto E, Shimaoka M, 2020. Integrin-ligand interactions in inflammation, cancer, and metabolic disease: insights into the multifaceted roles of an emerging ligand Irisin. Front. Cell Dev. Biol. 8, 588066 10.3389/fcell.2020.588066.

Polyzos SA, Anastasilakis AD, Efstathiadou ZA, Makras P, Perakakis N, Kountouras J, Mantzoros CS, 2018. Irisin in metabolic diseases. Endocrine 59 (2), 260–274. 10.1007/s12020-017-1476-1. [PubMed: 29170905]

Roca-Rivada A, Castelao C, Senin LL, Landrove MO, Baltar J, Belén Crujeiras A, Pardo M, 2013. FNDC5/irisin is not only a myokine but also an adipokine. PLoS One 8 (4), e60563. 10.1371/journal.pone.0060563. [PubMed: 23593248]

Roggia MF, Ueta T, 2015. αvβ5 integrin/FAK/PGC-1α pathway confers protective effects on retinal pigment epithelium. PLoS One 10 (8), e0134870. 10.1371/journal.pone.0134870. [PubMed: 26244551]

Ross RS, Borg TK, 2001. Integrins and the myocardium. Circ. Res 88 (11), 1112–1119. 10.1161/hh1101.091862. [PubMed: 11397776]

Sarrazy V, Koehler A, Chow ML, Zimina E, Li CX, Kato H, Hinz B, 2014. Integrins αvβ5 and αvβ3 promote latent TGF-β1 activation by human cardiac fibroblast contraction. Cardiovasc. Res 102 (3), 407–417. 10.1093/cvr/cvu053. [PubMed: 24639195]

Savill J, Dransfield I, Hogg N, Haslett C, 1990. Vitronectin receptor-mediated phagocytosis of cells undergoing apoptosis. Nature 343 (6254), 170–173. 10.1038/343170a0. [PubMed: 1688647]

Schnyder S, Handschin C, 2015. Skeletal muscle as an endocrine organ: PGC-1α, myokines and exercise. Bone 80, 115–125. 10.1016/j.bone.2015.02.008. [PubMed: 26453501]

Schumacher MA, Chinnam N, Ohashi T, Shah RS, Erickson HP, 2013. The structure of irisin reveals a novel intersubunit β-sheet fibronectin type III (FNIII) dimer: implications for receptor activation. J. Biol. Chem 288 (47), 33738–33744. 10.1074/jbc.M113.516641. [PubMed: 24114836]

Skoog P, Månsson J, Thorén P, 1985. Changes in renal sympathetic outflow during hypotensive haemorrhage in rats. Acta Physiol. Scand 125 (4), 655–660. 10.1111/j.1748-1716.1985.tb07768.x. [PubMed: 2418635]

Slate-Romano JJ, Yano N, Zhao TC, 2022. Irisin reduces inflammatory signaling pathways in inflammation-mediated metabolic syndrome. Mol. Cell. Endocrinol 552, 111676 10.1016/j.mce.2022.111676. [PubMed: 35569582]

Sui S, Hou Y, 2021. Dual integrin αvβ3 and αvβ5 blockade attenuates cardiac dysfunction by reducing fibrosis in a rat model of doxorubicin-induced cardiomyopathy. Scand. Cardiovasc. J 55 (5), 287–296. 10.1080/14017431.2021.1955960. [PubMed: 34296634]

Taga T, Suzuki A, Gonzalez-Gomez I, Gilles FH, Stins M, Shimada H, Laug WE, 2002. Alpha v-integrin antagonist EMD 121974 induces apoptosis in brain tumor cells growing on vitronectin and tenascin. Int. J. Cancer 98 (5), 690–697. 10.1002/ijc.10265. [PubMed: 11920637]

Torres LN, Torres Filho IP, Barbee RW, Tiba MH, Ward KR, Pittman RN, 2004. Systemic responses to prolonged hemorrhagic hypotension. Am. J. Physiol. Heart Circ. Physiol 286 (5), H1811–H1820. 10.1152/ajpheart.00837.2003. [PubMed: 14726303]

Tu TQ, Yin SG, Pang JW, Zhang XH, Zhang LF, Zhang YX, Jiang Y, 2021. Irisin contributes to neuroprotection by promoting mitochondrial biogenesis after experimental subarachnoid hemorrhage. Front. Aging Neurosci 13 10.3389/fnagi.2021.640215. Article 640215. [PubMed: 33613273]

Uhm JH, Dooley NP, Kyritsis AP, Rao JS, Gladson CL, 1999. Vitronectin, a glioma-derived extracellular matrix protein, protects tumor cells from apoptotic death. Clin. Cancer Res 5 (6), 1587–1594. [PubMed: 10389948]

Wang Z, Chen K, Han Y, Zhu H, Zhou X, Tan T, Zeng C, 2018. Irisin protects heart against ischemia-reperfusion injury through a SOD2-dependent mitochondria mechanism. J. Cardiovasc. Pharmacol 72 (6), 259–269. 10.1097/FJC.0000000000000608. [PubMed: 29979350]

Wang Y, Tian M, Tan J, Pei X, Lu C, Xin Y, Gong Y, 2022. Irisin ameliorates neuroinflammation and neuronal apoptosis through integrin αVβ5/AMPK signaling pathway after intracerebral hemorrhage in mice. J. Neuroinflammation 19 (1), 82. 10.1186/s12974-022-02438-6. [PubMed: 35392928]

Witzenbichler B, Kureishi Y, Luo Z, Le Roux A, Branellec D, Walsh K, 1999. Regulation of smooth muscle cell migration and integrin expression by the Gax transcription factor. J. Clin. Invest 104 (10), 1469–1480. 10.1172/JCI7251. [PubMed: 10562309]

Wolf AJ, Arruda A, Reyes CN, Kaplan AT, Shimada T, Shimada K, Underhill DM, 2011. Phagosomal degradation increases TLR access to bacterial ligands and enhances macrophage sensitivity to bacteria. J. Immunol 187 (11), 6002–6010. 10.4049/jimmunol.1100232. [PubMed: 22031762]

Wrann CD, White JP, Salogiannnis J, Laznik-Bogoslavski D, Wu J, Ma D, Spiegelman BM, 2013. Exercise induces hippocampal BDNF through a PGC-1α/FNDC5 pathway. Cell Metab 18 (5), 649–659. 10.1016/j.cmet.2013.09.008. [PubMed: 24120943]

Xiong XQ, Geng Z, Zhou B, Zhang F, Han Y, Zhou YB, Zhu GQ, 2018. FNDC5 attenuates adipose tissue inflammation and insulin resistance via AMPK-mediated macrophage polarization in obesity. Metab. Clin. Exp 83, 31–41. 10.1016/j.metabol.2018.01.013. [PubMed: 29374559]

Xu X, Zhang B, Wang Y, Shi S, Lv J, Fu Z, Song Q, 2023. Renal fibrosis in type 2 cardiorenal syndrome: an update on mechanisms and therapeutic opportunities. Biomed. Pharmacother 164, 114901 10.1016/j.biopha.2023.114901. [PubMed: 37224755]

Yano N, Zhang L, Wei D, Dubielecka PM, Wei L, Zhuang S, Zhao TC, 2020. Irisin counteracts high glucose and fatty acid-induced cytotoxicity by preserving the AMPK-insulin receptor signaling axis in C2C12 myoblasts. Am. J. Physiol. Endocrinol. Metab 318 (5), E791–E805. 10.1152/ajpendo.00219.2019. [PubMed: 32182124]

Yao Q, Liu J, Zhang Z, Li F, Zhang C, Lai B, Wang N, 2018. Peroxisome proliferator-activated receptor γ (PPARγ) induces the gene expression of integrin α. J. Biol. Chem 293 (43), 16572–16582. 10.1074/jbc.RA118.003161. [PubMed: 30181212]

Yun JH, Park SW, Kim JH, Park YJ, Cho CH, 2016. Angiopoietin 2 induces astrocyte apoptosis via αvβ5-integrin signaling in diabetic retinopathy. Cell Death Dis 7 (2), e2101 10.1038/cddis.2015.347. [PubMed: 26890140]

Zhu W, Sahar NE, Javaid HMA, Pak ES, Liang G, Wang Y, Huh JY, 2021. Exercise-induced Irisin decreases inflammation and improves NAFLD by competitive binding with MD2. Cells 10 (12). 10.3390/cells10123306.

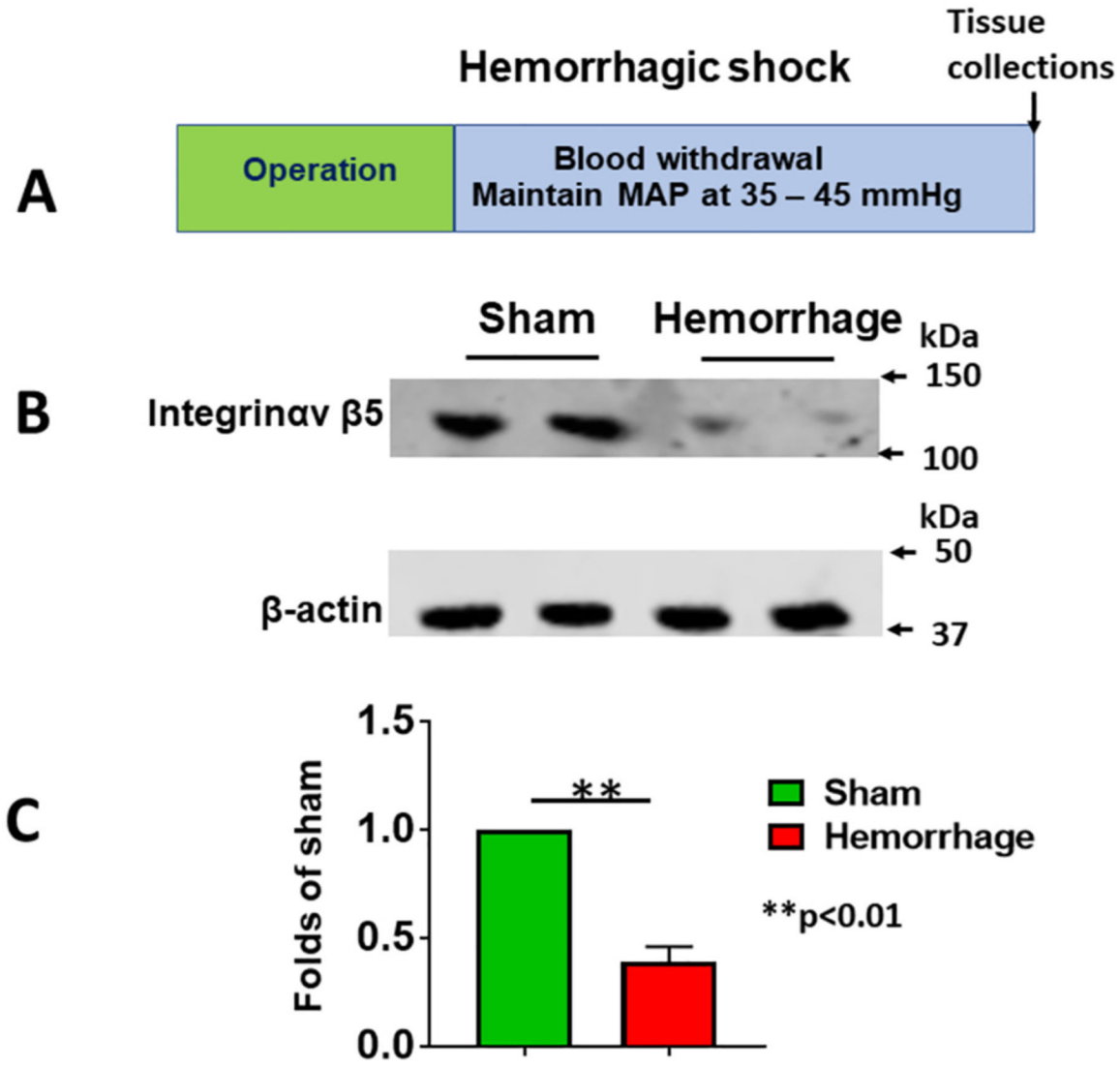

Fig. 1.

Hemorrhage resulted in the reduction of integrin αvβ5 protein in muscles. A: Hemorrhage protocol; B: Hemorrhage caused a decrease in integrin αvβ5; C: Densitometric analysis of integrin αvβ5 protein in muscle. Data are shown as Mean ± SEM (*n* = 3/each group); **p < 0.01.

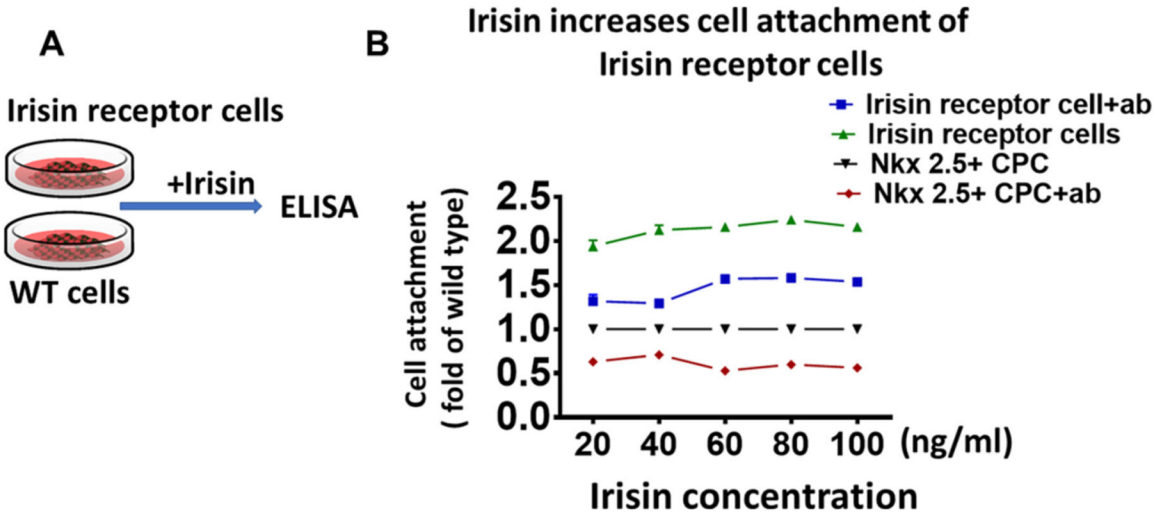

Figs. 2.

Binding of Irisin to integrin αvβ5 in vitro: A: Establishment of stable cell line overexpressing Integrin αvβ5 in embryonic stem cells (ESC)Nkx2.5^{+} cell. B: ELISA (Enzyme-linked immunosorbent assay) was performed to verify the direct binding of irisin binding to integrin αvβ5. Embryonic Nkx2.5+ESCs stable cells over-expressed integrin αvβ5 or wilt type cells were used to see the increased irisin binding to integrin αvβ5. The binding assay for detecting integrin αvβ5 and irisin were carried out using ELISA. Data are shown as Mean ± SEM, n = 5/each group.

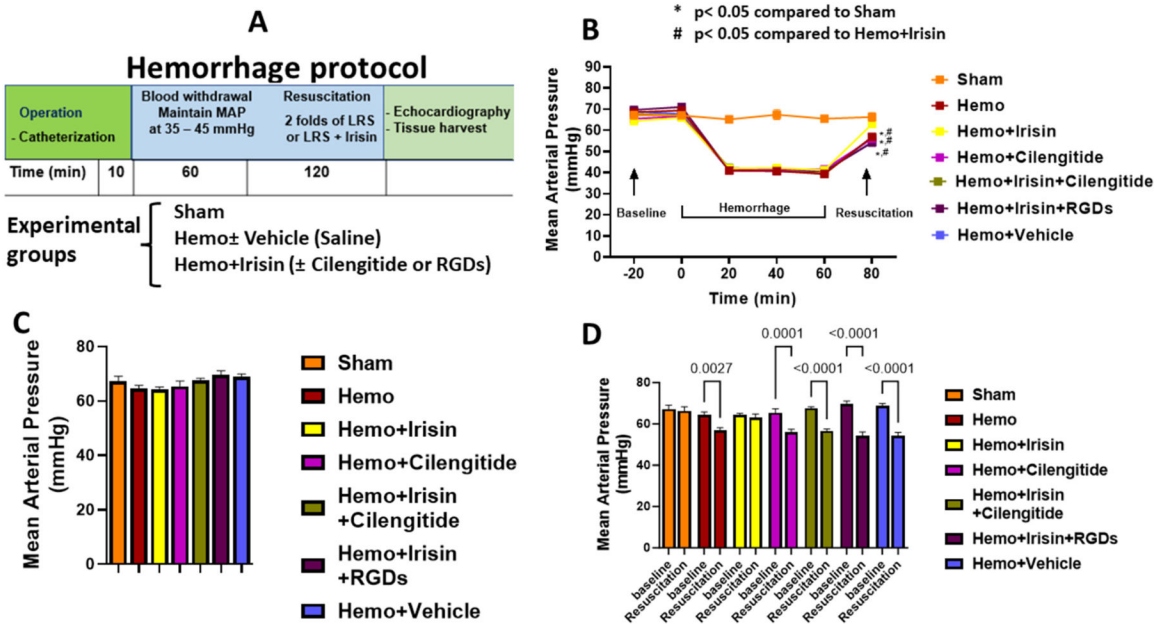

Fig. 3.

Time course and MAP during the hemorrhage. A: The protocol of hemorrhage and resuscitation: Mice were maintained MAP at 35–45 mmHg for one hour before resuscitation with lactated ringer's solution (LRS) in hemorrhagic shock groups; B: The time course of MAP during the hemorrhage; C: MAP prior to hemorrhage (Data are shown as Mean ± SEM, n = 5–7/each group); D: MAP of animals at baseline and at 20 min of resuscitation; Data are shown as Mean ± SEM, (n = 5–7/each group). MAP: Mean artery pressure; Hemo: Hemorrhage.

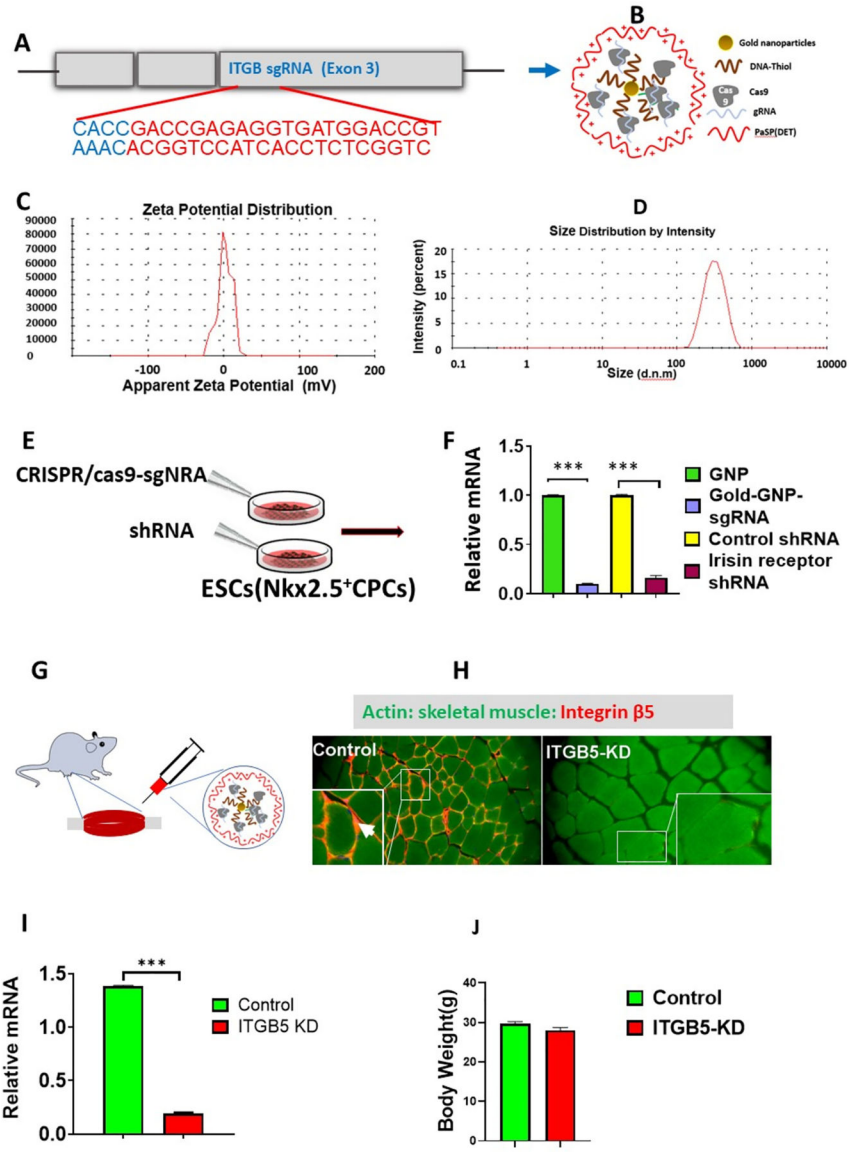

Fig. 4.

Characterization of Gold-CRISPR/Cas9-sgRNA delivery system. A: the sequence of sgRNA of integrin β-*5.* B: Gold-nano-CRISPR/Cas-9 delivery design and components; C: Stability assessment by measuring of zeta potential of CRISPR/Cas-9 sgRNA integrin β-*5* delivery with dynamic light scattering (DLS); D: Size distribution of CRISPR/Cas-9 sgRNA integrin β-*5;* E&F: In vitro knockdown of integrin β-*5* mRNA by Gold-CRISPR system and shRNA targeting integrin β-*5* in embryonic stem cells (Nkx2.5+ ESCs) (*n* = 5/per group). ***p < 0.001; G: Diagram of delivery Gold-CRISPR system was injected to mice and skeletal muscle was harvested at 2 weeks of delivery; H: Immunostaining detecting of *i*ntegrin β-*5.* I: mRNA of *i*ntegrin β-*5;* J: Body weight; Data were expressed as Mean ± SE (*n* = 4–5/per group).

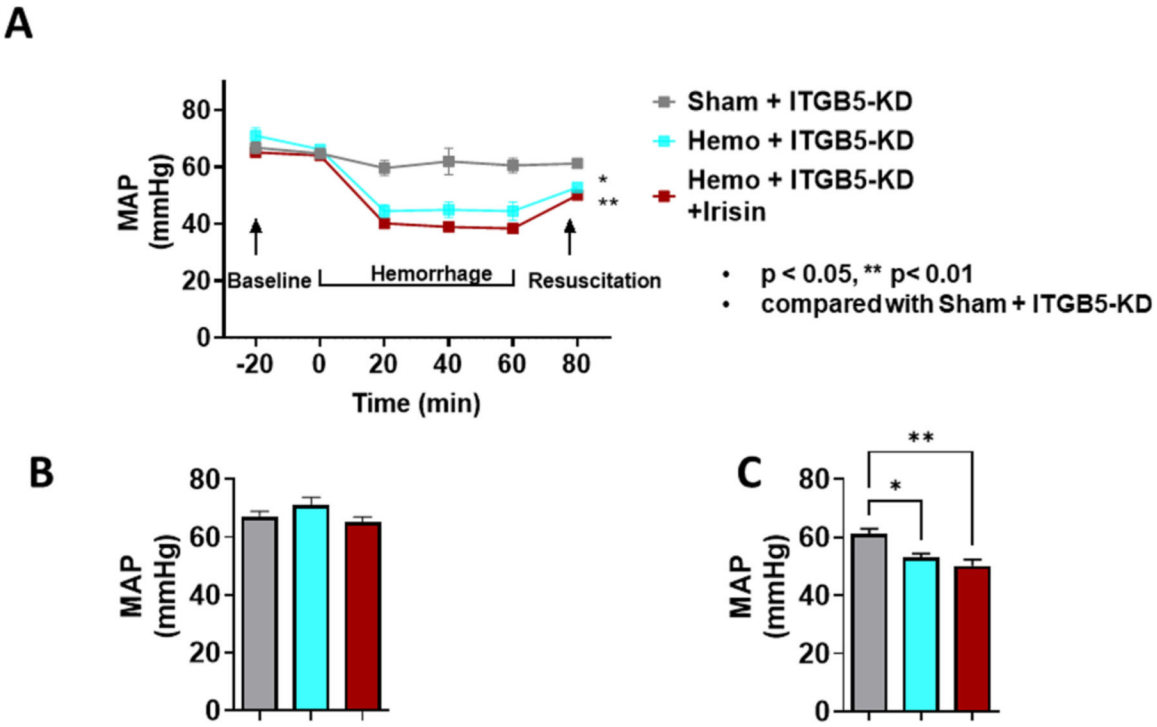

Fig. 5.

The MAP in mice exposed to hemorrhage following ITGB5 knockdown: Time course and MAP during the hemorrhagic shock period. A: The time course of MAP during the hemorrhage; B: MAP of animals before hemorrhage; C: MAP of animals at 20 min of resuscitation: Data are shown as Mean ± SEM (n = 4–6/each group), *p < 0.05; **p < 0.01. ITGB5: integrin β-*5.* KD: knockdown.

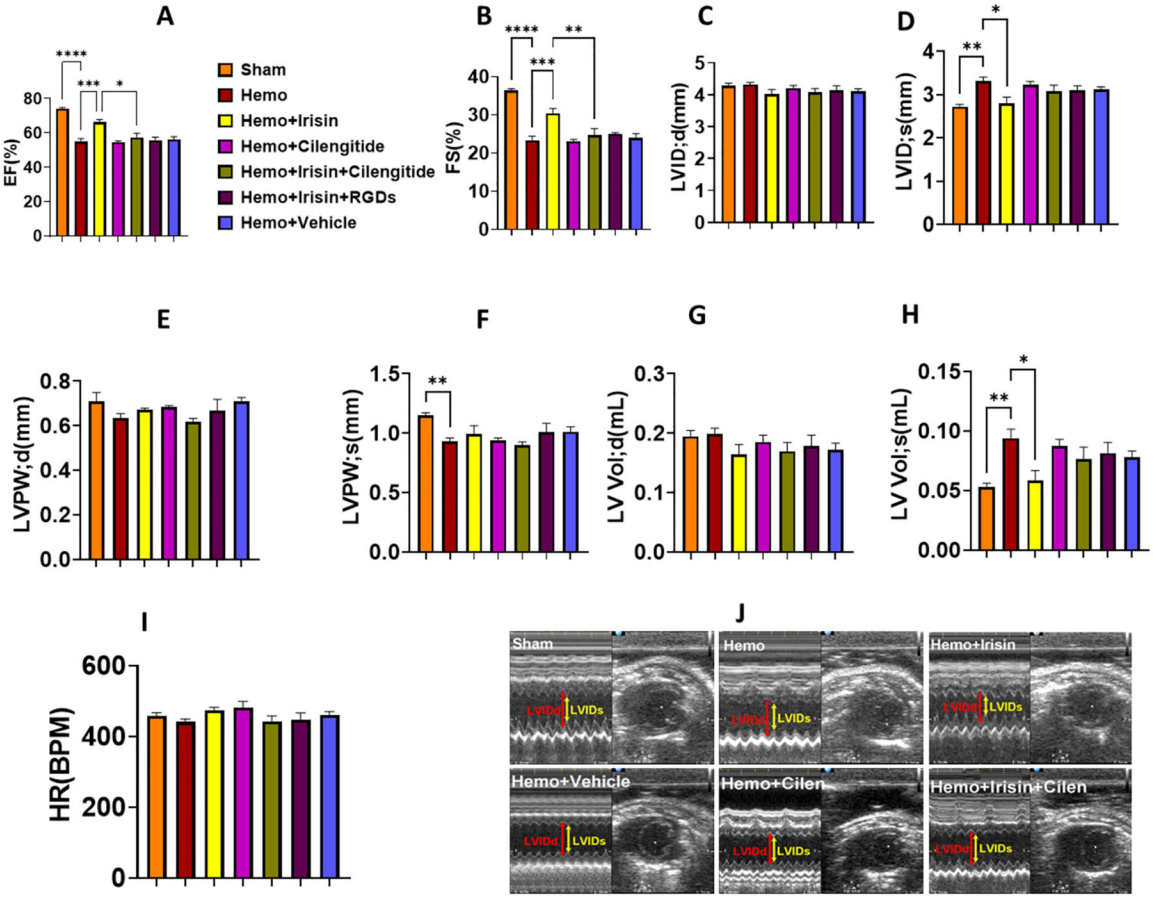

Fig. 6.

Echocardiographic metrics of cardiac function in hemorrhage. Left ventricular (LV) function were calculated using two-dimensional M mode in sham and hemorrhage groups 2 h after recovery from resuscitation. A: Ejection Fraction (EF); B: Fraction Shortening (FS); C: LV Internal Dimension in diastole (LVIDd); D: LV Internal Dimension in systole (LVIDs); E: LV Posterior Wall in diastole (LVPWd); F: LV Posterior Wall in systole (LVPWs); G: Left ventricular volume in systole (LVvol: d); H: Left ventricular volume in diastole (LVvol:s) I: Heart Rate (HR); J: Representative images of LV with B mode and M mode. Data are expressed as Mean ± SEM (n = 4–6/each group). *p < 0.05; **p < 0.01; ***p < 0.001; ****p < 0.0001.

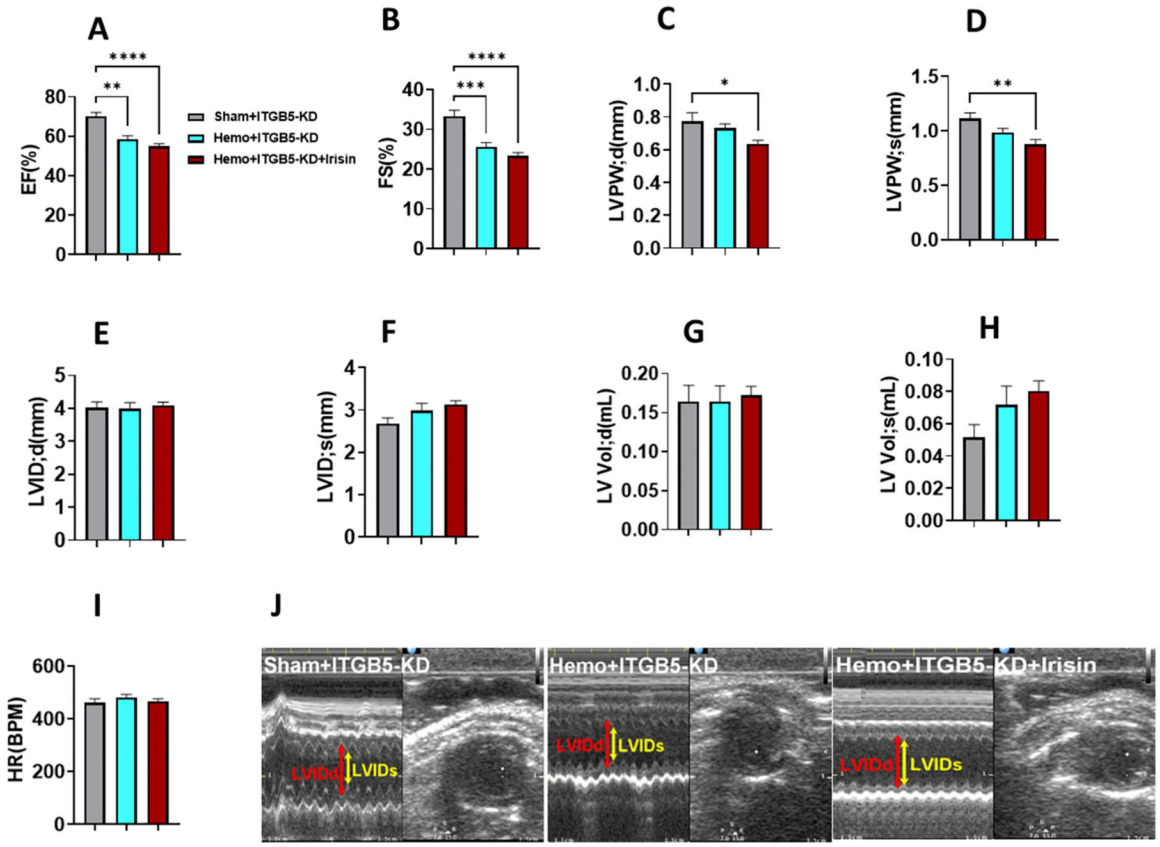

Fig. 7.

The cardiac function of mice exposed to hemorrhage following ITGB5 knockdown: A: EF; B: FS; C: LVPWd; D: LVPWs; E: LVIDd; F: LVIDs; G: LV vol,d; H: LV vol,s; I: HR; J: Representative images of LV with B mode and M mode. Data are expressed as Mean ± SEM (n = 4–6/each group), *p < 0.05, **p < 0.01, ***p < 0.001; ****p < 0.0001. The abbreviations are identical as the same in Fig. 6.

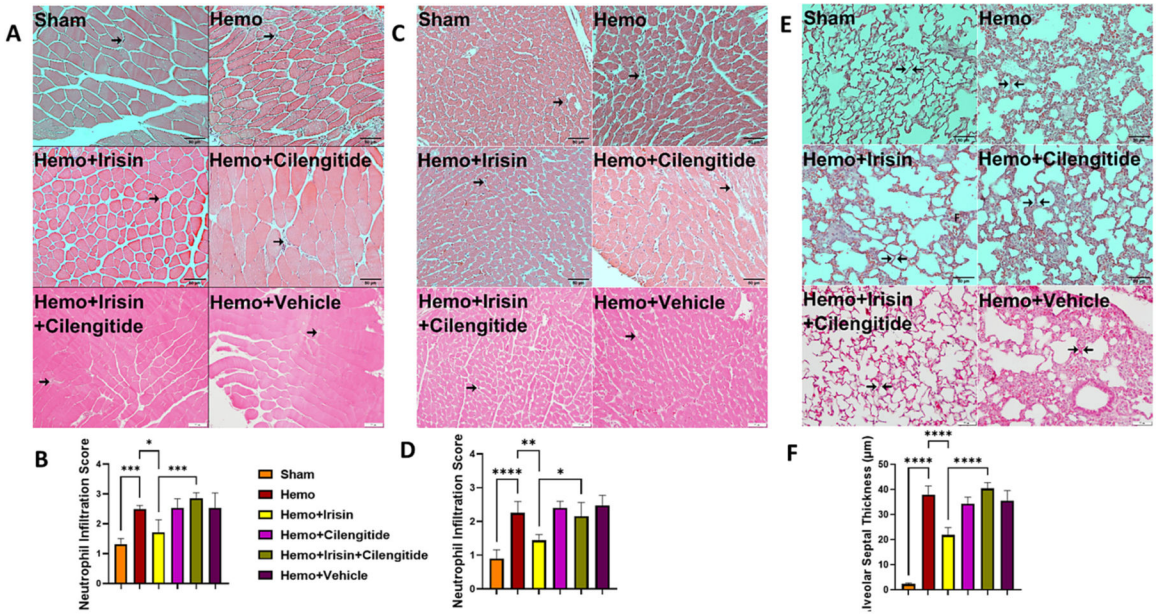

Fig. 8.

Histological analysis of injury in skeletal muscle, myocardium, and lung. A: Skeletal muscle histology (H&E staining) of sham operated, hemorrhagic group, and hemorrhagic-treated groups (200×, scale bars indicate 50 μm); B: A bar graph for data of inflammatory cell infiltration in skeletal muscle (Data are shown as Mean ± SEM, n = 5/each group); C: H&E staining of myocardium in sham operated, hemorrhagic groups, and hemorrhagic-treated groups (200×, scale bars indicate 50 μm); D: A bar graph for data of inflammatory infiltration in myocardium (Data are shown as Mean ± SEM, n = 5/each group); E: Histopathology by H&E staining of lungs in sham, hemorrhagic groups, and hemorrhagic-treated groups (200×, scale bars indicate 50 μm). Alveolar septal thickness was used to assess the extent of lung injury; F: A bar graph for data of alveolar septal thickness of the lung. Data are shown as Mean ± SEM (n = 5/each group); *p < 0.05; **p < 0.01; ***p < 0.001; ****p < 0.0001.

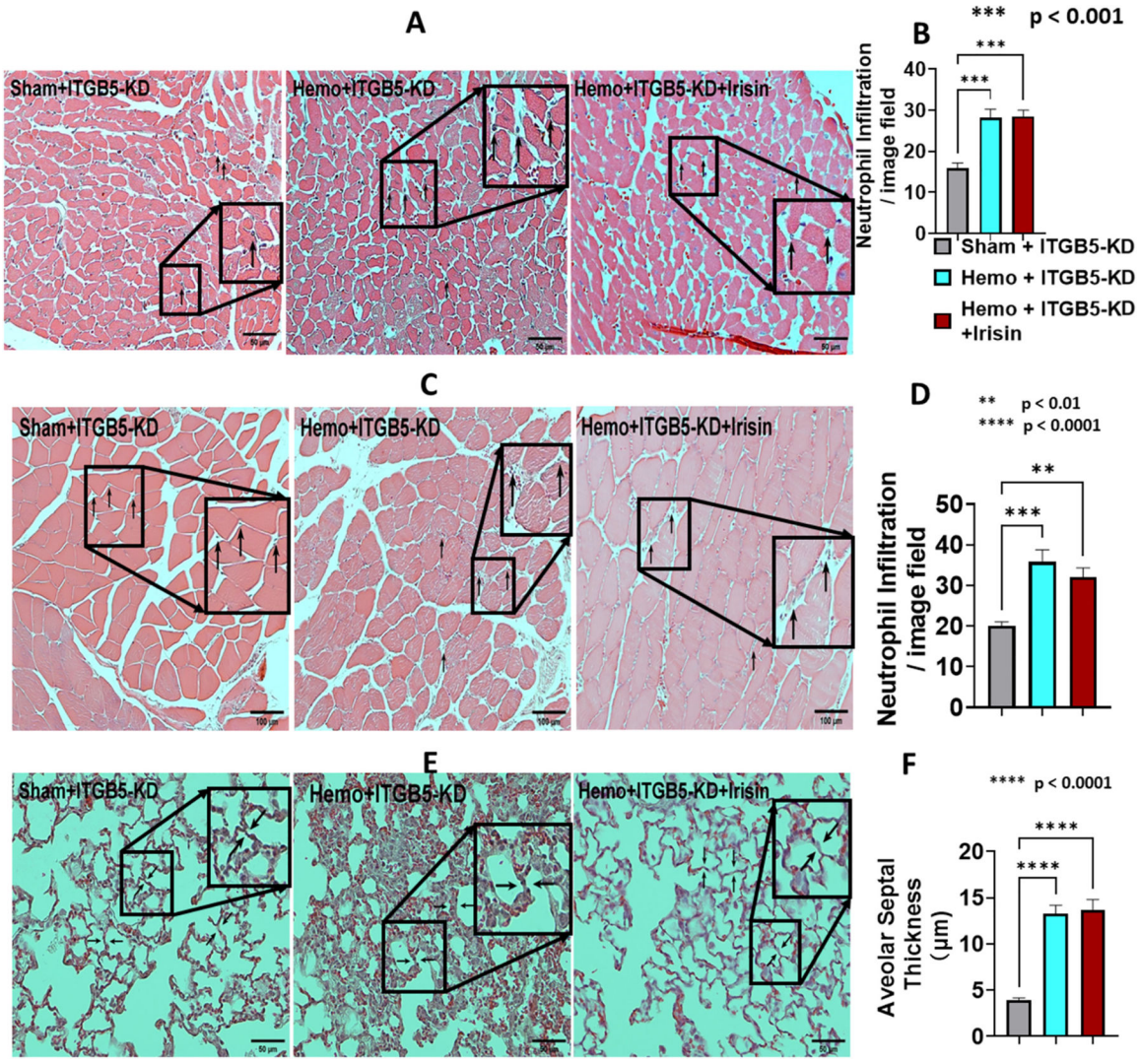

Fig. 9.

Histological analysis of pathological injury in skeletal muscle, myocardium, and lung tissues of the mice following ITGB5 knockdown. A: Myocardial histology (H&E staining) of sham operated, ITGB5 knockdown hemorrhage, and irisin-treated ITGB5 knockdown hemorrhage (scale bars indicate 50 μm); B: A bar graph for data of inflammatory cell infiltration in myocardium; C: H&E staining of skeletal muscle in sham operated, hemorrhagic group, and irisin-treated groups (scale bars indicate 100 μm); D: A bar graph for data of neutrophilic infiltration in skeletal muscle; E: H&E staining of lungs in sham operated, ITGB5 knockdown hemorrhage and irisin-treated ITGB5 knockdown hemorrhage (original magnification, scale bars indicate 50 μm). Alveolar septal thickness was used to assess the extent of lung injury; F: A bar graph for data of alveolar septal thickness of the lung. Data are shown as Mean ± SEM (n = 4–5/each group), **p < 0.01; ***p < 0.001; ****p < 0.0001.

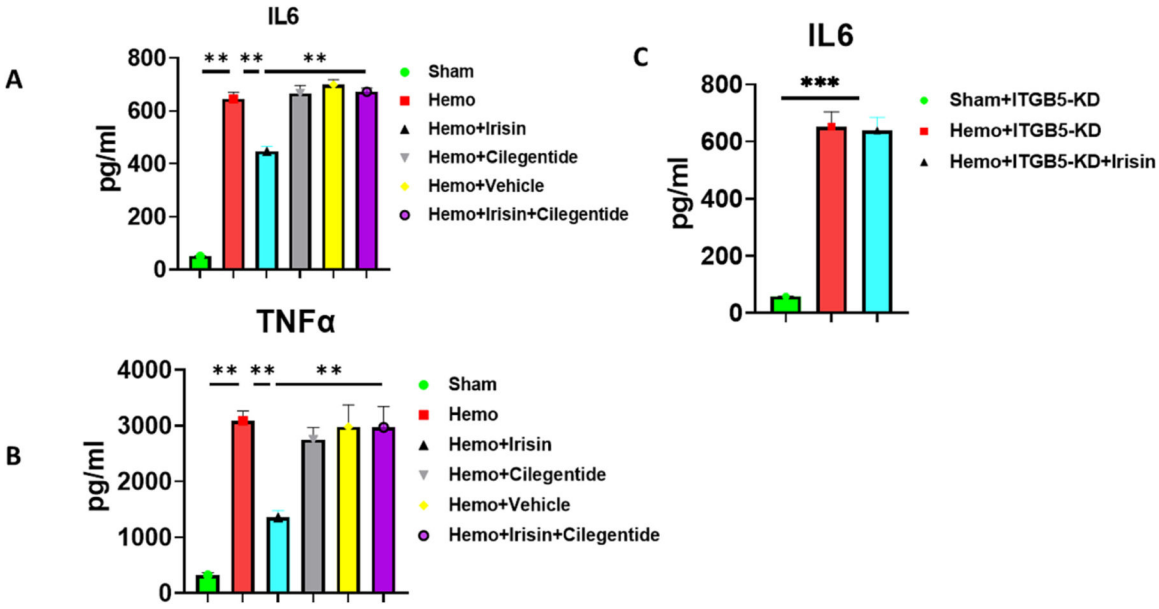

Fig. 10.

ELISA analysis of IL-6 and TNF-α in serum. Bar graphs for A: Levels of IL-6 in serum; B: Serum levels of TNF-α; Data are shown as Mean ± SEM (n = 5/each group). C: The cytokine release of mice exposed to hemorrhage following ITGB5 knockdown: ELISA analysis of IL-6 in serum among the groups, **p < 0.01; ***p < 0.001. Data are shown as Mean ± SEM (n = 4–6/each group).

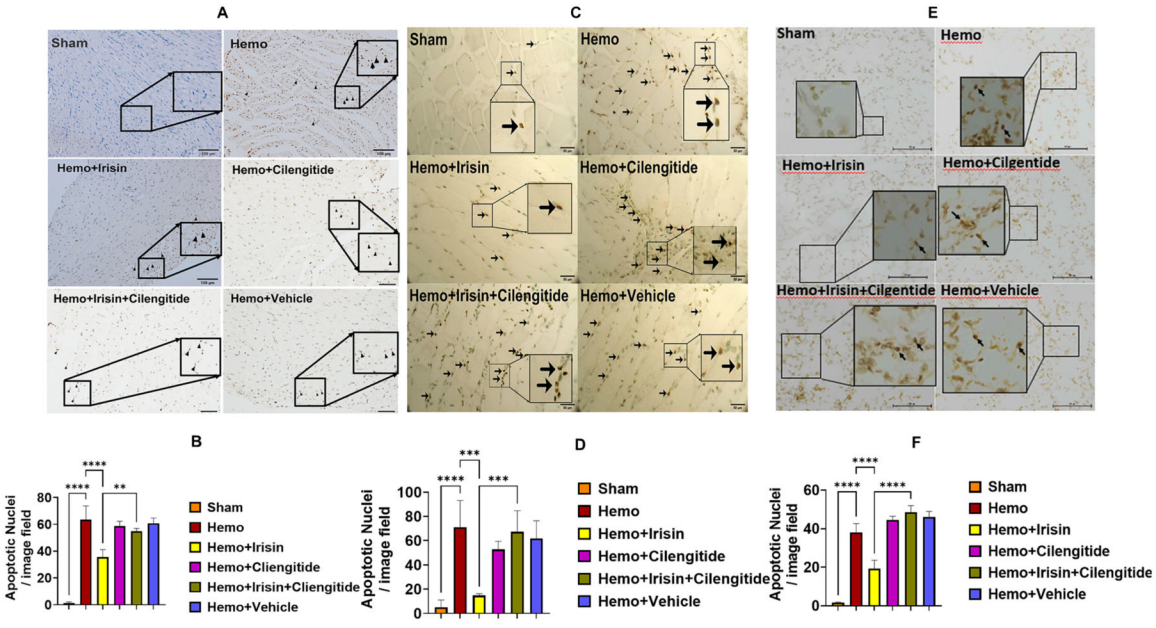

Fig. 11.

TUNEL staining of apoptosis in myocardium, skeletal muscle and lung following Cilengitide treatment. A: The image of apoptosis positive nuclei in myocardium (scale bar 100 μm). B: A bar graph for statistical data of apoptosis positive nuclei in myocardium. C: The image of apoptosis positive nuclei in skeletal muscle (scale bar 50 μm). D: A bar graph for statistical data of apoptosis positive nuclei in skeletal muscle. E: The Images of apoptosis positive nuclei in lung (scale bar 100 μm). F: A bar graph for statistical data of apoptosis positive nuclei in lung. Data are expressed as Mean ± SEM (n = 3–6/each group), **p < 0.01; ***p < 0.001; ****p < 0.0001.

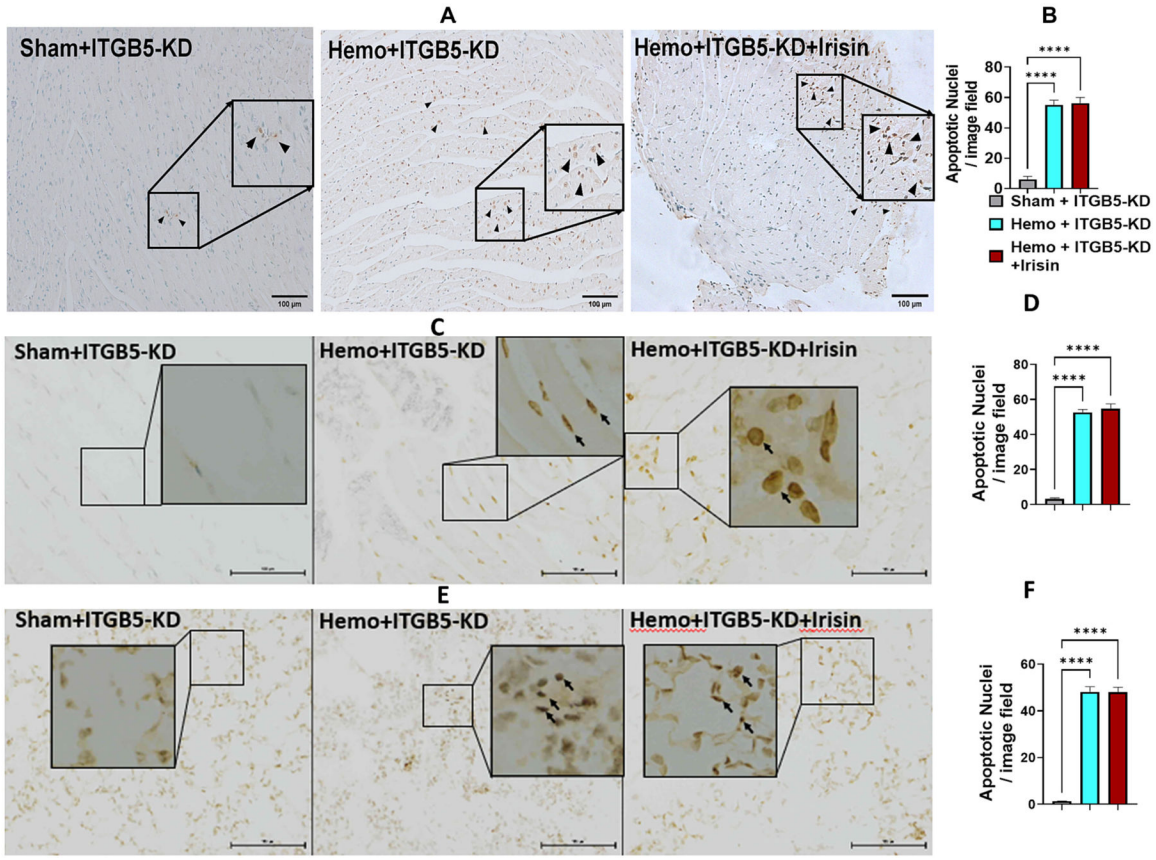

Fig. 12.

TUNEL staining of apoptosis in myocardium, skeletal muscle and lung following ITGB5 knockdown: A: The image of TUNEL positive nuclei in myocardium; B: A bar graph for statistical data of TUNEL in myocardium; C: The number of TUNEL positive nuclei in skeletal muscle (scale bar 100 μm). D: A bar graph for statistical data of TUNEL positive nuclei in skeletal muscle. E: The number of TUNEL positive nuclei in lung (scale bar 100 μm). F: A bar graph for statistical data of TUNEL positive nuclei in Lung. Data are expressed as Mean ± SEM (n = 4–6/each group); ****p < 0.0001.

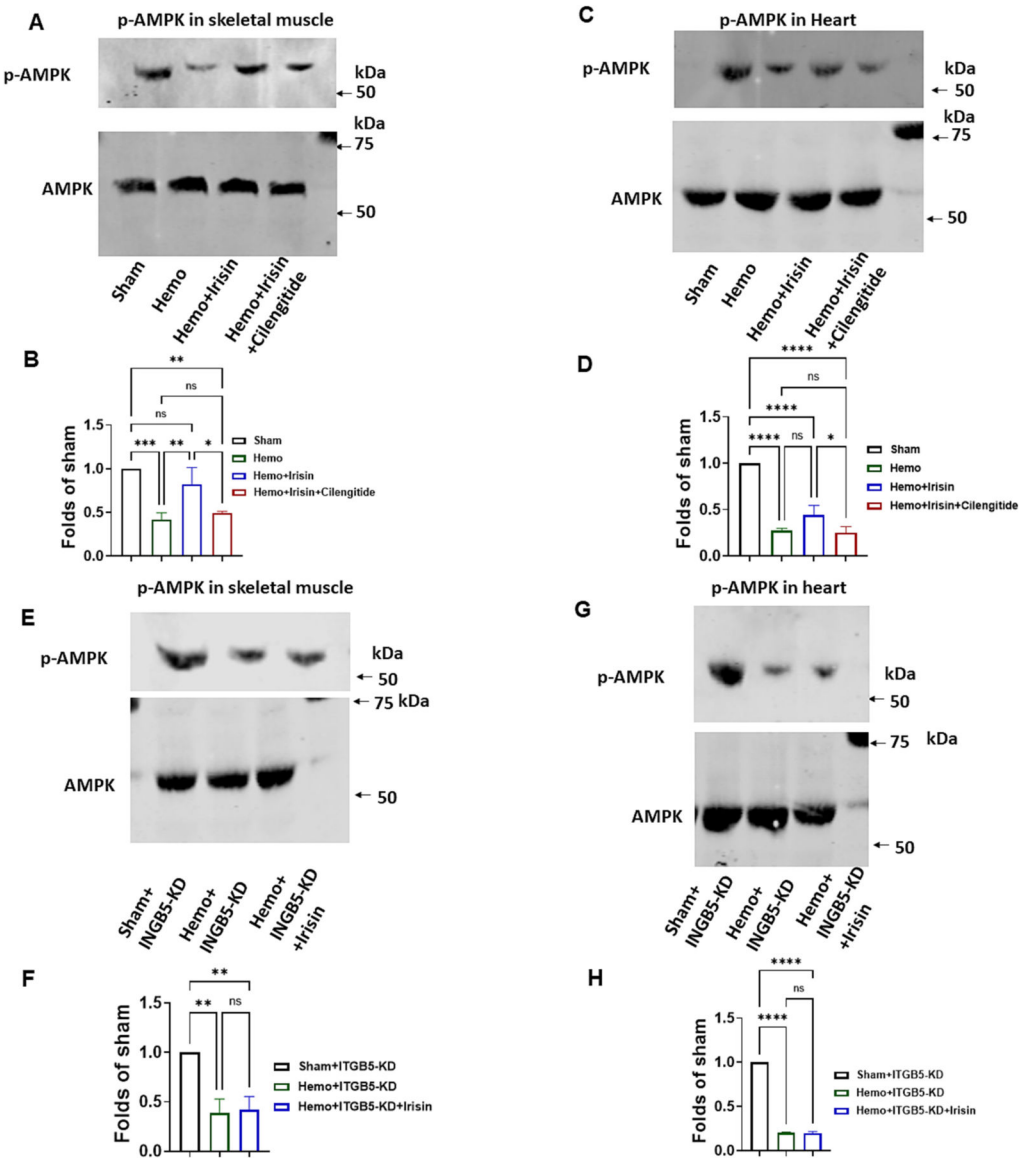

Fig. 13.

Western blot examines that AMPK phosphorylation in skeletal muscles and myocardium in ITGB5 sgRNA treatment. A: Phosphorylated-AMPK determined by Western blot in skeletal muscle of hemorrhage; B: A bar graph for densitometric analysis of p-AMPK. C: Phosphorylated-AMPK in myocardium; D: A bar graph for densitometric analysis of p-AMPK; E: Phosphorylated-AMPK in skeletal muscle in ITGB5 sgRNA treatment; F: A bar graph for densitometric analysis of p-AMPK. G: Phosphorylated-AMPK in myocardium of hemorrhage in ITGB5 sgRNA treatment; H: A bar graph for densitometric analysis of p-AMPK. Data are expressed as Mean ± SEM (n = 3/each group). *p < 0.05; **p < 0.01; ***p < 0.001; ****p < 0.0001.